ornl

OAK RIDGE NATIONAL LABORATORY

LOCKHEED MARTIN

ORNL/GWPO-026

Effective Porosity and Density of Carbonate Rocks (Maynardville Limestone and Copper Ridge Dolomite) within Bear Creek Valley on the Oak Ridge Reservation Based on Modern Petrophysical Techniques

J. Dorsch
Environmental Sciences Division

MANAGED AND OPERATED BY
LOCKHEED MARTIN ENERGY RESEARCH CORPORATION
FOR THE UNITED STATES
DEPARTMENT OF ENERGY

ORNL/GWPO-026

EFFECTIVE POROSITY AND DENSITY OF CARBONATE ROCKS (MAYNARDVILLE LIMESTONE AND COPPER RIDGE DOLOMITE) WITHIN BEAR CREEK VALLEY ON THE OAK RIDGE RESERVATION BASED ON MODERN PETROPHYSICAL TECHNIQUES

J. Dorsch

Environmental Sciences Division, Oak Ridge National Laboratory, Oak Ridge, TN 37831-6400

Date Issued--February, 1997

Prepared by the
Environmental Sciences Division
Oak Ridge National Laboratory

Prepared for
Groundwater Program Office
under budget and reporting code EU2010301

OAK RIDGE NATIONAL LABORATORY
Oak Ridge, Tennessee 37831-6285
managed by
LOCKHEED MARTIN ENERGY RESEARCH CORPORATION
for the
US DEPARTMENT OF ENERGY
under contract DE-AC05-96OR22464

Table of Contents

FIGURES

TABLES

ACKNOWLEDGMENTS

RaNaye Dreier and Bradley J. Carr are thanked for critically reading a previous draft of this report which resulted in improvements. Any shortcomings, however, remain the responsibility of the author. The support from the Y-12 HSE&A-Division, administered through Joe A. Johnston, Jr. and David B. Watson is most gratefully acknowledged. The research was supported in part by an appointment to the Oak Ridge National Laboratory Postdoctoral Research Associates Program (awarded to J. Dorsch) administered jointly by the Oak Ridge National Laboratory and the Oak Ridge Institute for Science and Education.

EXECUTIVE SUMMARY

Helium porosimetry and the immersion-saturation technique were applied to obtain modern petrophysical data for limestone and dolostone specimens from the Copper Ridge Dolomite and Maynardville Limestone (coreholes GW-131, GW-135; Bear Creek Valley) on the Oak Ridge Reservation (ORR). These modern petrophysical data, including effective porosity, specimen bulk- and grain-density, will find use for groundwater-flow and contaminant-flow modeling in the vicinity of the Y-12 Plant, will be important to evaluate the possible extent of matrix diffusion within the fractured carbonate aquifer, and will provide quantitative parameters for geophysical modeling on the ORR.

Effective porosity values range from 0.06% to 8.13% (helium porosimetry) and from 0.14% to 4.52% (immersion-saturation technique). The vast majority of values are <2% with a distinct mode centered on the 0.3% class. Limestone specimens display effective porosity values <1%, whereas dolostone specimens may display such low values but, more commonly, display values >>1%. Highest effective porosity values are encountered within the Copper Ridge Dolomite (middle to lower part of the analyzed section) and within the middle part of zone 6 of the Maynardville Limestone. There is a drastic drop in effective porosity toward the lower part of zone 6 and the lower zones of the Maynardville Limestone. This change reflects the increase in well cemented limestone at the expense of dolostone with secondary porosity. Noteworthy is, furthermore, that intervals with vuggy porosity can display higher effective porosity values, but that this is not the rule indicating that the larger pores may not be well connected.

Comparison to effective porosity data generated by Goldstrand et al. (1995) revealed that for higher effective porosity intervals (dolostone) effective porosity was systematically underestimated by Goldstrand et al. (1995). This observation is most likely explained by insufficient saturation time and the use of inaccurate bulk-density values. For lower effective porosity intervals (mostly limestone) effective porosity values generally compare more favorable, although for 25% of the comparison intervals effective porosity as reported by Goldstrand et al. (1995) is (significantly) higher.

Specimen grain-density data range from 2.70 to 2.87 $g \cdot cm^{-3}$ and display a bimodal distribution, which reflects the mineralogy (calcite, dolomite) of the specimens. Specimen bulk-density data range from 2.62 to 2.83 $g \cdot cm^{-3}$, which is significantly narrower than earlier reported data indicating potential problems with the methodology used by Goldstrand et al. (1995).

PURPOSE

The purpose of this study is to provide quantitative data on effective porosity of carbonate rock from the Maynardville Limestone and Copper Ridge Dolomite within Bear Creek Valley based on modern petrophysical techniques. The data will be useful for groundwater-flow and contaminant-flow modeling in the vicinity of the Y-12 Plant on the Oak Ridge Reservation (ORR). Furthermore, the data provides needed information on the amount of interconnected pore space potentially available for operation of matrix diffusion as a transport process within the fractured carbonate rock. A second aspect of this study is to compare effective porosity data based on modern petrophysical techniques to effective porosity data determined earlier by Goldstrand et al. (1995) with a different technique. An added bonus of the study is quantitative data on the bulk density and grain density of dolostone and limestone of the Maynardville Limestone and Copper Ridge Dolomite which might find use for geophysical modeling on the ORR.

INTRODUCTION

Specimens of carbonate rock from the Maynardville Limestone and Copper Ridge Dolomite from the Whiteoak Mountain thrust sheet on the Oak Ridge Reservation (ORR) were analyzed. Petrophysical analyses were conducted using helium porosimetry and the immersion-saturation method. Petrophysical data obtained with the laboratory experiments include effective porosity ("matrix porosity"), specimen grain-density and specimen bulk-density. The data are expected to contribute to the ongoing hydrological investigations within Bear Creek Valley in the vicinity of the Y-12 Plant, especially the modeling of groundwater flow and contaminant transport.

Maynardville Limestone and Copper Ridge Dolomite within Bear Creek Valley on the ORR

Stratigraphy. The Maynardville Limestone and Copper Ridge Dolomite are carbonate units which constitute the lower part of the regional Knox aquifer (Figure 1; Solomon et al., 1992). The two formations are Upper Cambrian in age (e.g., Rodgers, 1953) and formed part of the extensive Cambro-Ordovician carbonate bank which developed upon the passive continental margin of Laurentia bordering the evolving Iapetus ocean (Rodgers, 1969; Bird and Dewey, 1970; Read, 1989). Maynardville Limestone and the Copper Ridge Dolomite are contained within the Whiteoak Mountain and Copper Creek thrust sheets and traverse the ORR as two narrow bands (Figure 2). The contact between the two formations is described as gradational (Dreier et al., 1992).

The Maynardville Limestone is the uppermost formation of the Conasauga Group (Figure 1) and reaches a thickness of 117 to 137 m within Bear Creek Valley (Dreier et al., 1992; Shevenell et al., 1993). The unit is generally described as massive to thinly bedded, light gray to tan, thrombolitic, oolitic, and peloidal limestone; algal laminated and stromatolitic dolostone increases in abundance upward within the formation (Goldstrand, 1995). The Maynardville Limestone is thought to have been deposited in shallow-marine subtidal to intertidal environments and, to a smaller extent, in supratidal environments (Weber, 1988; Goldstrand, 1995).

The Copper Ridge Dolomite is the lowermost formation of the Knox Group (Figure 1) and reaches a thickness of 74 to 102 m within Bear Creek Valley (Hatcher et al., 1992b). It is described to consist of massive to thinly bedded, tan to medium gray

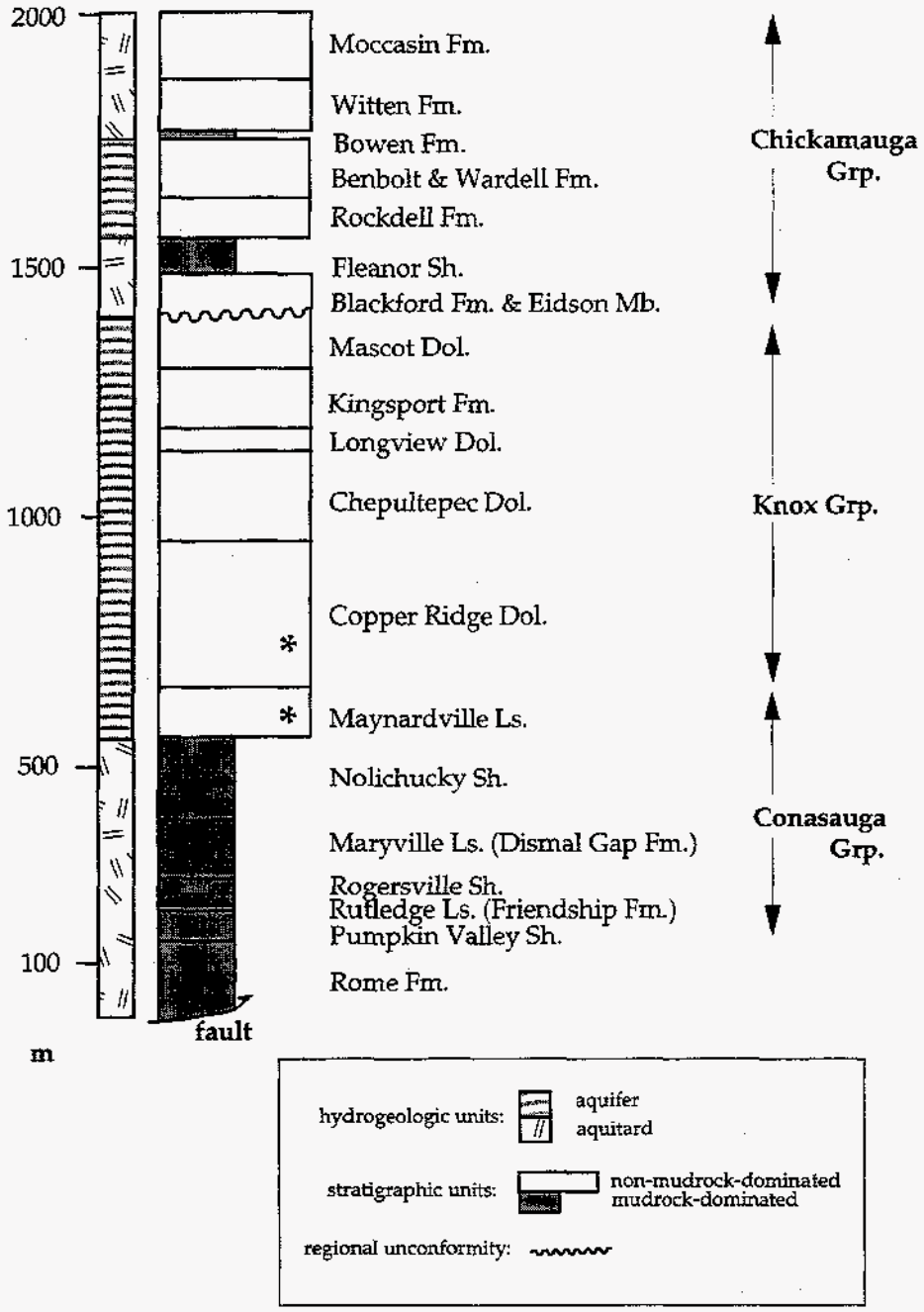

Fig. 1: Stratigraphic section for the Copper Creek and Whiteoak Mountain thrust sheets on the ORR. Thickness values (in m) are averages of measured stratigraphic thicknesses. Thickness data and distribution of aquifer and aquitard hydrostratigraphic units are derived from Hatcher et al. (1992a). The star highlights the Copper Ridge Dolomite (lower to middle) and the Maynardville Limestone which were sampled for petrophysical measurements within Bear Creek Valley (modified from Dorsch, 1995).

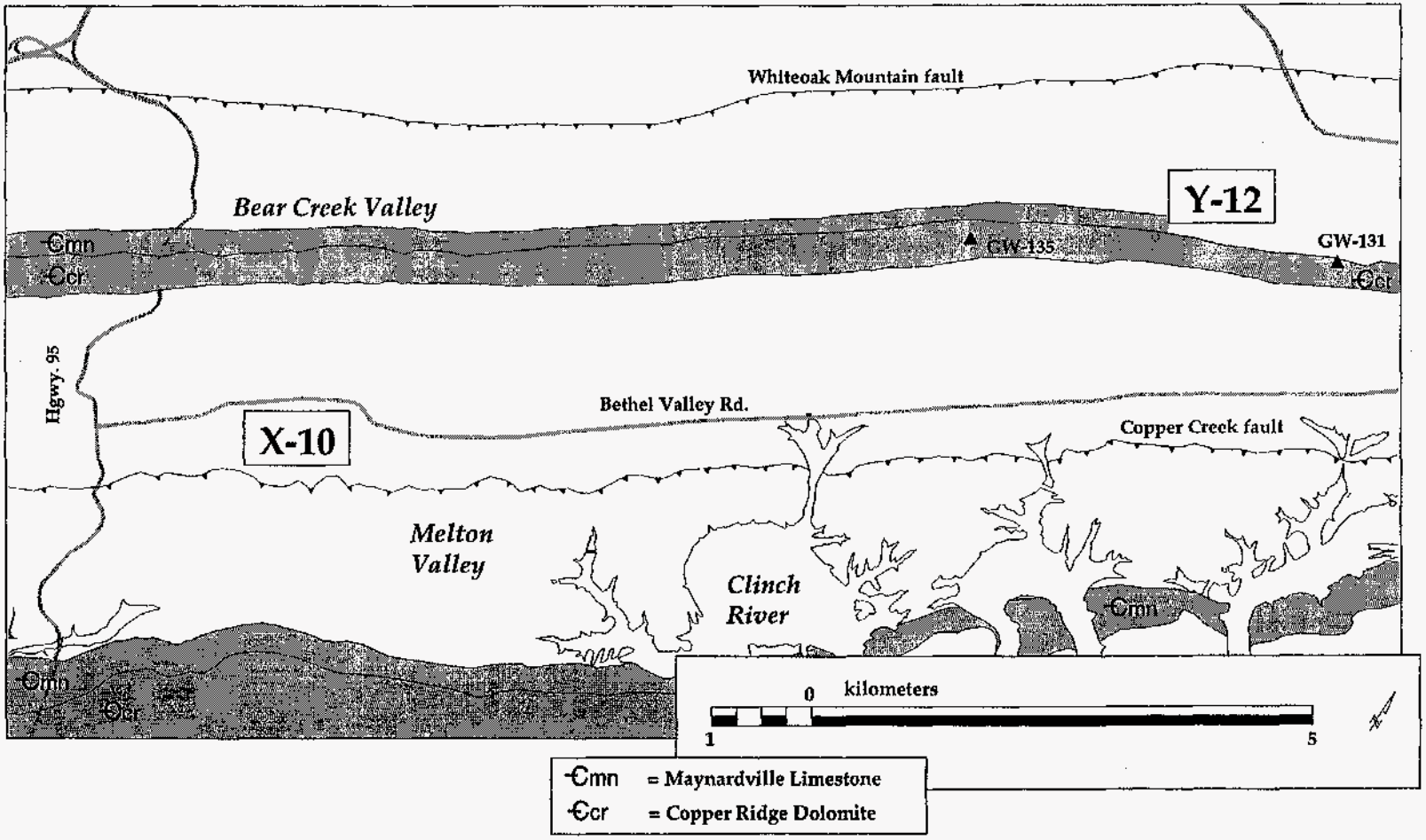

Fig. 2: Generalized location map. Dark stippled bands traversing the ORR outline the carbonate rock of the Copper Ridge Dolomite and of the Maynardville Limestone (note that the units are not continuously mapped throughout the ORR). Barbed solid black lines indicate the location of the Whiteoak Mountain fault and of the Copper Creek fault, whereas the stippled lines indicate major roads. Triangles refer to the location of coreholes from which specimens were selected: corehole GW-131 and GW-135 (based on Hatcher et al., 1992a).

dolostone, which contains abundant stylolites and is locally rich in chert (King and Haase, 1987; Hatcher et al., 1992b). The depositional environments are interpreted as shallow subtidal to supratidal (Lee and Ketelle, 1987; Weber, 1988).

The Maynardville Limestone can be subdivided into the Low Hollow Member (lower part of the Maynardville Limestone) and the Chances Branch Member (upper part of the Maynardville Limestone) (Miller and Fuller, 1954; Hasson and Haase, 1988; Dreier et al., 1992). Based on the analysis of gamma-ray geophysical logs, Shevenell et al. (1993) subdivided the Maynardville Limestone within Bear Creek Valley on the ORR into seven zones. Zone 1 corresponds to the uppermost Nolichucky Shale; zones 2 and 3 correspond, respectively, to the lower and upper Low Hollow Member, whereas zones 4, 5, and 6 correspond to the lower, middle and upper Chances Branch Member, respectively (Shevenell et al., 1993; Goldstrand, 1995). Commonly, zone 7 is only difficult to identify lithologically and geophysically, and is therefore incorporated into zone 6 (Goldstrand, 1995).

The Copper Ridge Dolomite exhibits a repetitive stratigraphic motif of asymmetric, laterally continuous, 1 to 4 m thick cycles composed of 3 lithofacies types (Lee and Ketelle, 1987). The fine-grained, shaly and cryptalgal laminated dolostone of lithofacies 1 is prone to weathering at depth and exhibits fracturing which provides stratabound pathways for groundwater flow (Lee and Ketelle, 1987).

Goldstrand (1995) provides extensive lithologic descriptions coupled with gamma-ray geophysical logs of cores obtained from the Maynardville Limestone (and its zones) and the Copper Ridge Dolomite within Bear Creek Valley. Furthermore, Goldstrand (1995) summarizes the abundant stratigraphic data from the Maynardville Limestone using isopach maps and stratigraphic cross sections.

Diagenesis and Porosity. Some observations on the diagenetic history of the Maynardville Limestone and the Copper Ridge Dolomite are provided by Saunders and Toran (1994), Goldstrand (1995), and Goldstrand et al. (1995). Based on petrographic examination, Goldstrand (1995) concluded that all primary porosity within the Maynardville Limestone is occluded, and that the present porosity is all secondary in origin. Four factors are listed as the primary controls on secondary porosity development within the Maynardville Limestone and Copper Ridge Dolomite (Goldstrand, 1995; Goldstrand et al., 1995): 1) dissolution of anhydrite and gypsum is responsible for vuggy porosity within the Maynardville Limestone and Copper Ridge Dolomite; vugs can reach several cm in length (Saunders and Toran, 1994; Goldstrand,

1995; Goldstrand et al., 1995); 2) dedolomitization (e. g., the calcification of dolostone through dissolution of dolomite mineral-matter concomitant with precipitation of calcite [e. g., Füchtbauer and Richter, 1988]) caused secondary porosity within the dolomitic parts of the Maynardville Limestone and Copper Ridge Dolomite; it is responsible for abundant interconnected micropores and the development of moldic porosity (Goldstrand, 1995; Goldstrand et al., 1995); dedolomitization was aided by the dissolution of gypsum which provided added Ca^{2+} ions for calcite precipitation (Saunders and Toran, 1994); in addition to authigenic calcite, predominantly in vugs caused by the dissolution of gypsum and anhydrite, authigenic barite and celestite was formed (Saunders and Toran, 1994); 3) carbonate grain-size is an influencing factor in that smaller grains (i.e., carbonate mud) with larger surface areas favor dissolution; dissolution of carbonate mud caused fenestral and vuggy porosity, especially associated with stromatolitic and thrombolitic intervals (Goldstrand, 1995; Goldstrand et al., 1995); 4) oxidation of sulfide minerals, such as pyrite, and their dissolution is another cause for the development of moldic porosity (Goldstrand, 1995; Goldstrand et al., 1995). In addition, there is also abundant evidence for the dissolution of calcite and dolomite (Saunders and Toran, 1994) at shallow depths and the development of karst features throughout the dipping strata of the Maynardville Limestone and Copper Ridge Dolomite (Goldstrand and Shevenell, 1994; Goldstrand, 1995; Goldstrand et al., 1995).

Quantitative data on effective porosity of carbonate rock from the Maynardville Limestone and Copper Ridge Dolomite are reported by Goldstrand et al. (1995) and Goldstrand (1995). Overall, the carbonate units appear "tight," with an average "matrix porosity" of 0.8 % for the Maynardville Limestone and 1.3% for the Copper Ridge Dolomite (Goldstrand et al., 1995). Porosities tend to decrease with depth for all coreholes, with the lower Copper Ridge Dolomite and zone 6 of the Maynardville Limestone providing the highest values in effective porosity, followed by zone 5.

Effective porosity was determined in the laboratory (Goldstrand et al., 1995) using a water-immersion technique similar to the one used in this study (see chapter on *Petrophysical Techniques*). Two aspects of the chosen methodology, however, give rise to questions concerning the generated effective porosity data: 1) a sample bulk-density of 2.65 $g \cdot cm^{-3}$ was assumed for all carbonate-rock samples; this value is unlikely to be correct for (Paleozoic) limestone and dolostone samples based on published compilations (e. g., Olhoeft and Johnson, 1989); 2) a vacuum-saturation period of 30 min was used which, most likely, is not long enough to ensure complete saturation of the carbonate-rock sample with water; a test performed by Goldstrand et al. (1995) at the

conclusion (?) of the laboratory experiments showed that maximum saturation of some carbonate-rock samples was accomplished only after a vacuum-saturation period of 2 h. The result of both methodological aspects will be to underestimate the effective porosity of Maynardville Limestone and Copper Ridge Dolomite carbonate facies. Goldstrand et al. (1995) recommended a further examination of the effective porosity of these carbonate facies using more sophisticated petrophysical measurement techniques.

PETROPHYSICAL MEASUREMENT TECHNIQUES

Petrophysical data (effective porosity, specimen grain-density, specimen bulk-density) for carbonate-rock specimens were obtained using state-of-the-art laboratory-based measurement techniques. These techniques include helium porosimetry and the immersion-saturation method. Both of these techniques generated petrophysical data using a specimen size of 37 g or less.

Immersion-Saturation Method

Principle. The immersion-saturation method is based on determining the difference in specimen weight between the fully saturated state and the dry state of the specimen. Re-saturation of the specimen with a liquid (deionized water) is assumed to penetrate all of the interconnected pore space (Katsube et al., 1992a; Katsube, 1992).

Effective Porosity. Effective porosity can be calculated by:

$$\phi_I = \delta_r \left[(W_w - W_d) / W_d \cdot \delta_w \right] , \qquad (1)$$

where ϕ_I = effective porosity (determined with the Immers.-Sat. Method);
δ_r = bulk density of the rock specimen;
W_w = sample weight wet;
W_d = sample weight dry;
δ_w = bulk density of water.

Procedure. The following analytical procedural steps for the immersion-saturation method were followed during the experiments (Figure 3). The procedure corresponds to the one employed at the Geological Survey of Canada (Katsube and Scromeda, 1991; Katsube et al., 1992b; Scromeda and Katsube, 1993, 1994; N. Scromeda-Perez, pers. comm. 1995) and the one employed for the determination of effective porosity of Conasauga Group mudrock on the ORR (Dorsch et al., 1996). The sole modification is an increase in the time of vacuum degassing from 30 min to 2 h 15 min on day one of the experiment (Figure 3).

On *day one* of the experiment, the specimens, contained in dry glass beakers, were subjected to 15 minutes of vacuum degassing using a vacuum chamber and an applied vacuum ranging from 27 to 28.5 in Hg (68.6 to 72.4 cm). Following vacuum degassing, the hood of the vacuum chamber was removed and the specimens were submerged by filling the beakers with deionized water. Thereafter, the vacuum chamber was closed again and another period of vacuum degassing (for 2 h, at an applied

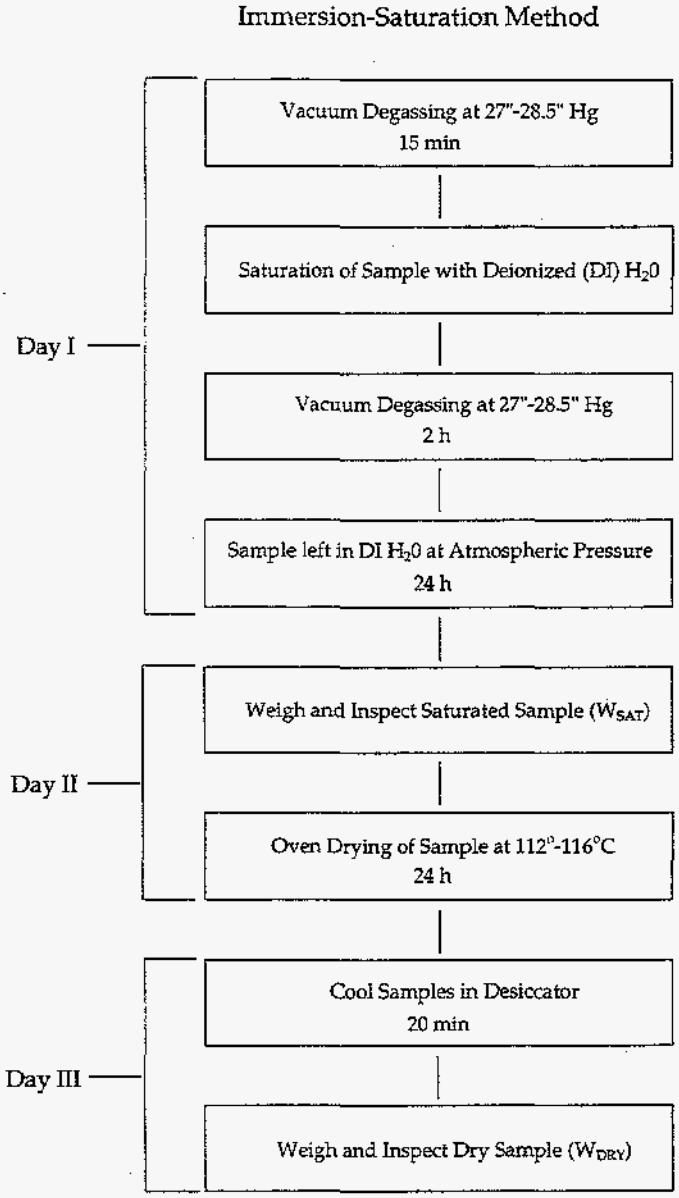

Fig. 3: Flow chart outlining the procedural steps for the immersion-saturation method as used in this study. Flow chart is based on the procedure employed at the Geological Survey of Canada (Katsube and Scromeda, 1991; Katsube et al., 1992; N. Scromeda-Perez, pers. comm., 1995) (modified from Dorsch et al., 1996).

vacuum between 27 to 28.5 in Hg) was administered. Day one concluded with removal of the water-filled specimen beakers from the vacuum chamber. The specimen beakers remained under atmospheric pressure for 24 h ensuring complete saturation of the specimens.

On *day two* of the procedure, one specimen at a time was carefully removed from the water-filled beaker and the water was discarded from the beaker. The specimen and the beaker were touched only with tweezers or a kimwipe® tissue. The surface of the specimen was carefully patted with a kimwipe® tissue to ensure that all surface water was removed from the specimen (no reflection sheen left), but avoiding to completely dry the surface. It is important to keep this drying process consistent for each specimen and to accomplish this task quickly. During this phase, the specimen was studied carefully for any irregularities, such as breakage. Thereafter, the specimen was weighed to determine the saturated weight (W_{SAT}). Specimen weights were recorded in g to the fourth decimal using a balance with a sensitivity of ±0.1 mg. Following weighing, the specimen was put back into an empty glass beaker and placed into an oven preheated to 112 to 116°C. The specimens remained in the oven at this temperature for 24 h to ensure complete drying of the specimens.

Day three of the procedure started with removing the specimens from the oven. The specimen beakers were quickly put into a desiccator and remained there shielded from the laboratory air for 20 min to cool. Then, one specimen beaker at a time was removed from the desiccator using tongs and weighed (see above). This step was accomplished quickly to avoid the specimen drawing moisture from the laboratory air. Following this, the specimen was removed from the glass beaker and the empty beaker was weighed. At this point the specimen was again carefully inspected for irregularities. The dry specimen weight (W_{DRY}) was determined by subtracting the weight of the beaker from the combined specimen and beaker weight.

Effective porosity of the specimens was calculated using formula (1). Data on the bulk density of the specimens were determined based on the mercury immersion-technique (see below).

Helium Porosimetry

Principle. Helium porosimetry is based on the Boyle-Mariotte Law. A change in gas volume or gas pressure causes a commensurate change in gas pressure or volume, given that the temperature remains constant. Important for helium porosimetry is that

an increase in available space causes the gas to expand resulting in the decrease in gas pressure (American Petroleum Institute, 1960; Luffel and Howard, 1988).

Procedure. Prior to the petrophysical measurements, the specimens were placed into soxhlet-type extractors and cleaned using a methyl alcohol solvent. Following cleaning, the specimens were dried in a vacuum oven at a temperature of 60°C for 24 h. Following oven drying the specimens were cooled in a desiccator.

For helium porosimetry the specimen is placed into a steel chamber of known volume. Helium isothermally expands into the chamber from a reservoir of known volume and pressure until equilibrium pressure is reached. From the new gas pressure the grain volume can be calculated. The bulk volume of the sample is then determined using a Archimedes mercury immersion-technique (see below)[1].

Effective Porosity. Effective porosity is calculated by subtracting the grain volume from the bulk volume, and dividing the result by the bulk volume of the specimen:

$$\phi_{He} = (V_{bimm} - V_g) / V_{bimm} , \qquad (2)$$

where ϕ_{He} = effective porosity (determined with helium porosimetry);
V_g = grain volume;
V_{bimm} = bulk specimen-volume measured with the mercury immersion-technique.

The values obtained with helium porosimetry are considered to reflect the total interconnected pore space (effective porosity) of a specimen.

Specimen Densities. Specimen densities were determined during the course of helium porosimetry. Specimen grain-density is obtained by dividing the weight of the specimen by the grain volume of the specimen (as determined through helium porosimetry, see above):

$$\delta_{grain} = W_{samp} / V_g , \qquad (3)$$

where δ_{grain} = specimen grain-density;
W_{samp} = weight of specimen.

[1] The experiments involving helium porosimetry and the Archimedes mercury immersion-technique were performed by *Core Petrophysics, Inc.* (contact: Robert A. Easterly; 6849 East 13th Street, Tulsa, Oklahoma 74112).

Sample bulk-density is obtained by weighing the specimen prior to immersion in mercury and then dividing the mass of the specimen by the bulk volume of the specimen (as determined by Archimedes mercury immersion-technique, see footnote 1):

$$\delta_{bulk} = W_{samp} / V_{bimm} , \qquad (4)$$

where δ_{bulk} = specimen bulk-density.

Specimen bulk-volume is determined by using the submerged weight of the specimen (difference in weight of a container filled with mercury before and after immersion of the specimen) and dividing it by the density of mercury:

$$V_{bimm} = W_{subm} / \delta_{Hg} , \qquad (5)$$

where W_{subm} = submerged weight of specimen;
δ_{Hg} = density of mercury.

SAMPLING

Cores

Carbonate-rock specimens (dolostone, limestone) for the petrophysical measurements were obtained from coreholes drilled into the Whiteoak Mountain thrust sheet on the ORR. The drill sites are situated within Bear Creek Valley (Figure 2) along strike of the Y-12 Plant. Core material was available from coreholes GW-131 and GW-135 (Figure 4). The cores are complete and are stored in Building 7042 ('core barn') at X-10 for inspection.

Sampling Intervals

The cores were inspected and sampling intervals were selected (Appendix I). Selection criteria were: 1) coverage of the different zones of the Maynardville Limestone; 2) coverage of sampling intervals used by Goldstrand (1995) for porosity determination and petrographic analysis (core GW-135); and 3) inclusion of some of the vuggy lithologies within the lower Copper Ridge Dolomite. A sampling interval is generally 9 cm (3.5 in) in length and provided a set of specimens for petrophysical analysis. The code for the sampling intervals includes the corehole designation followed by an interval number (e. g., GW-131-44) which refers to the core-box number. Two sampling intervals were chosen from core boxes 49 and 69 from core GW-131; then, the interval number is followed by the suffix -1 or -2. Appendix I provides an overview of sampling intervals, their code, drill depth (the median depth of the chosen sampling interval), and the stratigraphic unit which was sampled. Overall, 50 sampling intervals were selected from cores GW-131 and GW-135.

Specimens

Specimens for petrophysical analysis were selected from the chosen sampling intervals. The sampling intervals provided core segments approximately 3.5 in long, which were sawed into three disks of 1 in thickness each using a trim saw with tap water as coolant. Core plugs were drilled from the 1 in disks at the University of Tennessee Engineering Machine Shop using a drill press with a 1 in inner diameter diamond coring-bit and tap water as coolant. Ninety-five core plugs of 1 in length and 1 in diameter were finally available. One of the core plugs from each sampling interval

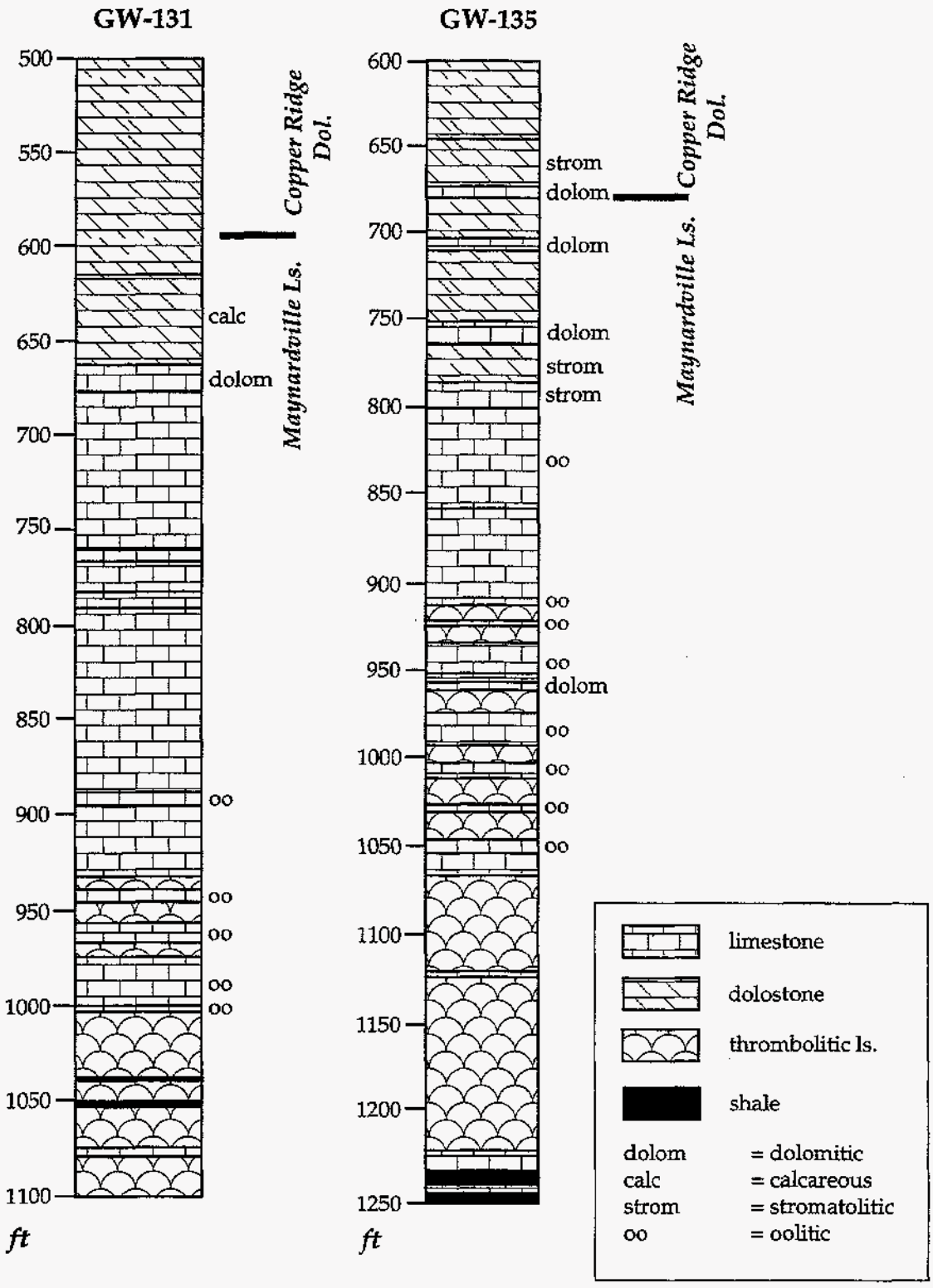

Fig. 4: Stratigraphic sections of coreholes GW-131 and GW-135 based on core inspection of Goldstrand (1995). Depth is in feet below ground surface (modified from Goldstrand, 1995).

was used for helium porosimetry (specimens with the suffix -A) for a total of 50. Ten of the core plugs were used for the immersion-saturation method (specimens with the suffix -B).

The remaining 35 core plugs were taken to obtain 70 disks of 1 in diameter and a thickness of 0.5 in by using a trim saw with tap water as coolant. Thirty-five of these disks were analyzed using the immersion-saturation method (specimens with the suffix -C).

Finally, box-shaped specimens were sawed from sampling-interval discs using a trim saw with tap water as coolant. Fifteen of the box-shaped specimens were analyzed with the immersion-saturation method (specimens with the suffix -D).

Specimens with the suffix -A or -B (core plugs) weighed between 35 g and 37 g. Specimens with the suffix -C (core-plug disks) weighed between 14 g and 16 g (with one specimen weighing 18.4 g), whereas specimens with the suffix -D (box shapes) weighed between 12.6 g and 16 g.

PETROPHYSICAL DATA AND DISCUSSION

Specimen Density-Data

Specimen density-data are available from all 50 sampling intervals. Specimen bulk-density data were obtained based on the Archimedes mercury immersion-technique, whereas specimen grain-density data were determined during helium porosimetry (see chapter on *Petrophysical Techniques*). The values of specimen bulk-density and grain-density for the Maynardville Limestone and the Copper Ridge Dolomite from coreholes GW-135 and GW-131 are summarized in Appendix II; Appendix III provides an overview of calculated statistical measures (note that some statistical measures are based on a small number of samples).

Specimen Bulk-Density. Specimen bulk-density data display an arithmetic mean of 2.74 (±0.04) $g \cdot cm^{-3}$ based on all measurements. The values range from a maximum of 2.83 $g \cdot cm^{-3}$ to a minimum of 2.62 $g \cdot cm^{-3}$. The minimum value, however, clearly is an outlier with all other values being >2.68 $g \cdot cm^{-3}$ (Fig. 5). The scatter within the data set is displayed in Figure 6. The arithmetic means for GW-131 and GW-135 data are nearly the same. There is, however, a decrease in value for both coreholes from the Copper Ridge Dolomite (bulk density arithmetic mean of 2.78 $g \cdot cm^{-3}$) to the Maynardville Limestone and its different zones (bulk density arithmetic mean <2.75 $g \cdot cm^{-3}$). Some of the Maynardville Limestone zones from corehole GW-135 display higher arithmetic means than equivalent zones from corehole GW-131.

Specimen Grain-Density. The values of grain-density range from a minimum of 2.70 $g \cdot cm^{-3}$ to a maximum of 2.87 $g \cdot cm^{-3}$, with an arithmetic mean of 2.77 (±0.06) $g \cdot cm^{-3}$ based on all measurements. There is a distinct bimodality exhibited by the data set (Fig. 7), with one mode centered on the 2.71 $g \cdot cm^{-3}$ class and the second mode centered on the 2.83 $g \cdot cm^{-3}$ class. The scatter within the data set is shown in Figure 8. The arithmetic means of the data from GW-131 and GW-135 are identical. As was the case for the bulk-density data, however, there is a distinct decrease in grain-density value from the Copper Ridge Dolomite (grain density arithmetic mean 2.83 to 2.82 $g \cdot cm^{-3}$), to zone 6 of the Maynardville Limestone (grain density arithmetic mean 2.79 to 2.77 $g \cdot cm^{-3}$), and then to the remaining zones of the Maynardville Limestone (grain density arithmetic mean <2.75 $g \cdot cm^{-3}$). The arithmetic means of the different zones of the

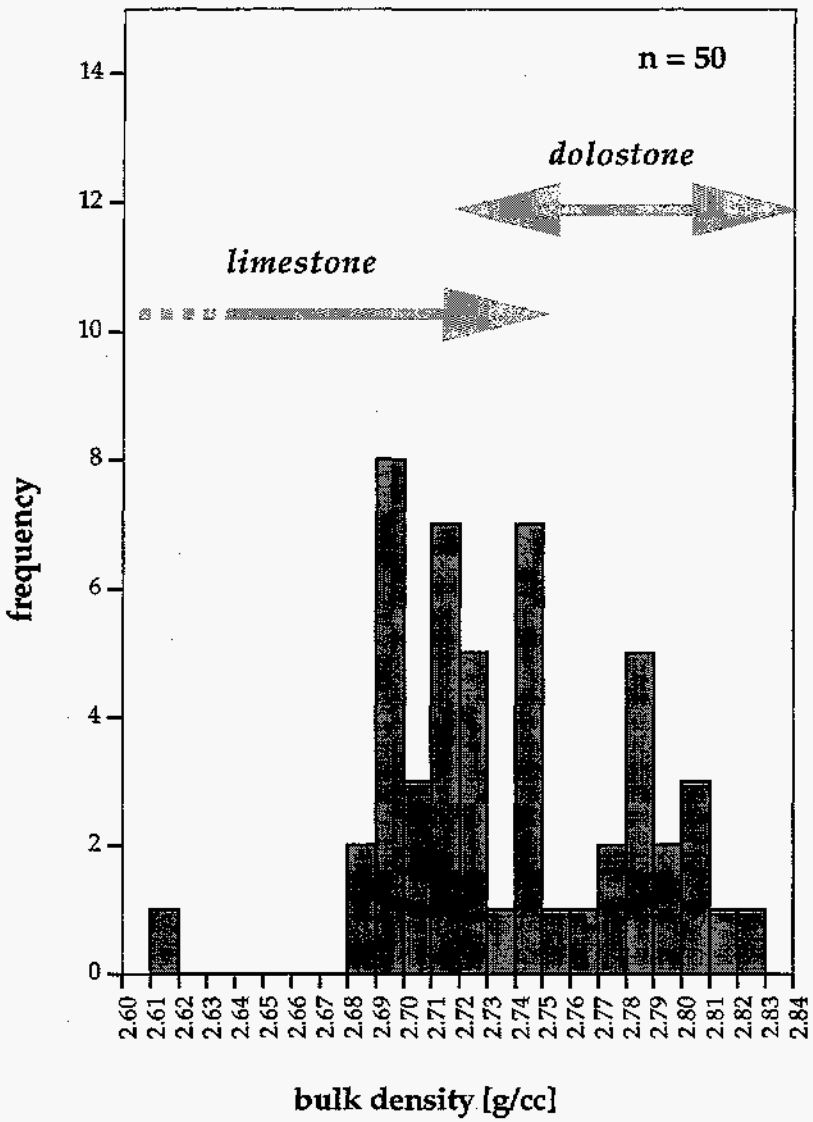

Fig. 5: Frequency distribution of bulk-density data for carbonate rocks of the Maynardville Limestone and Copper Ridge Dolomite (Bear Creek Valley, ORR) based on mercury immersion. Arrows indicate the range of bulk densities of limestone and dolostone as provided by Olhoeft and Johnson (1989).

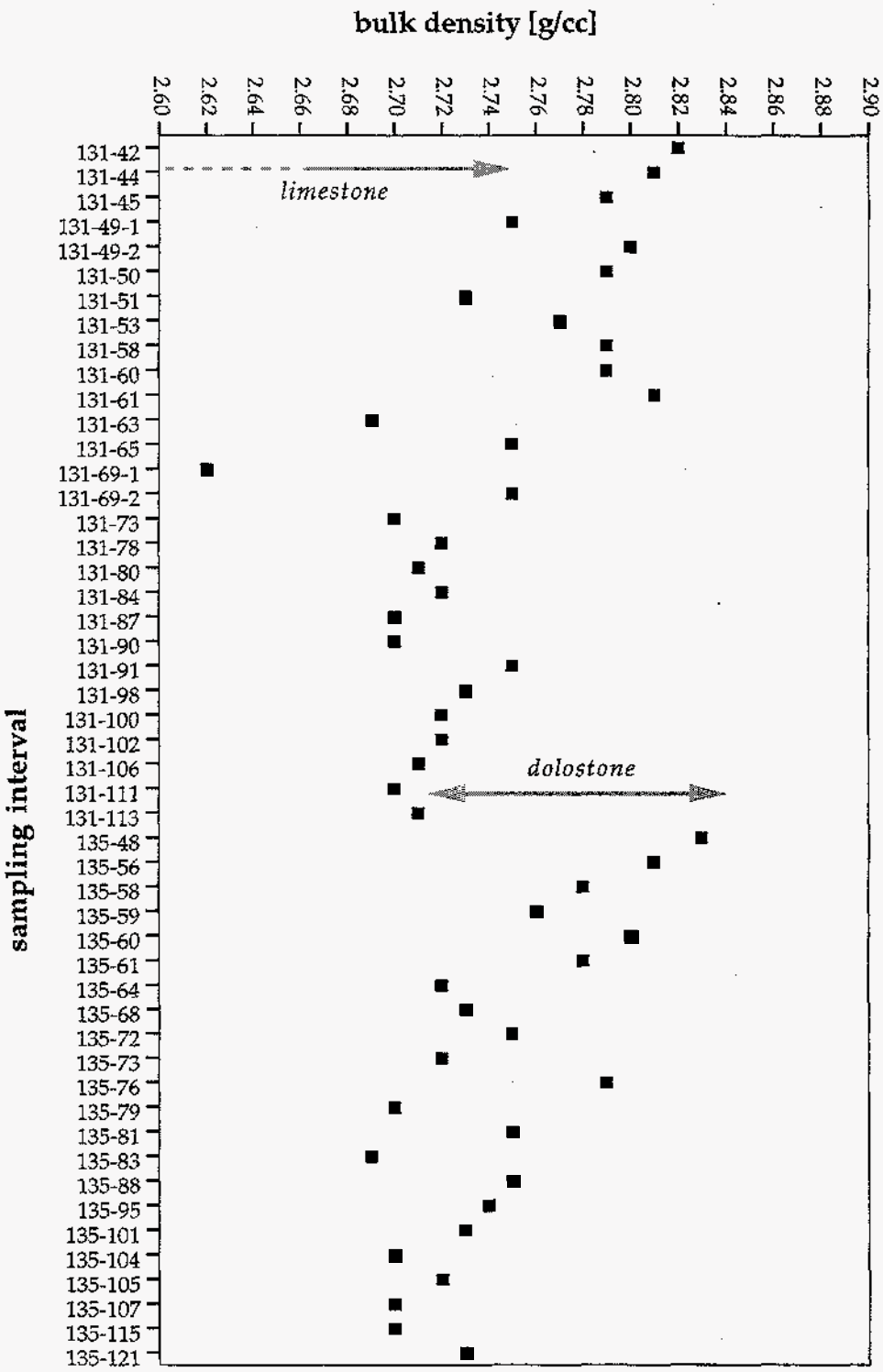
bulk density [g/cc]
2.60
2.62
2.64
2.66
2.68
2.70
2.72
2.74
2.76
2.78
2.80
2.82
2.84
2.86
2.88
2.90
sampling interval
131-42
131-44
131-45
131-49-1
131-49-2
131-50
131-51
131-53
131-58
131-60
131-61
131-63
131-65
131-69-1
131-69-2
131-73
131-78
131-80
131-84
131-87
131-90
131-91
131-98
131-100
131-102
131-106
131-111
131-113
135-48
135-56
135-58
135-59
135-60
135-61
135-64
135-68
135-72
135-73
135-76
135-79
135-81
135-83
135-88
135-95
135-101
135-104
135-105
135-107
135-115
135-121
limestone
dolostone

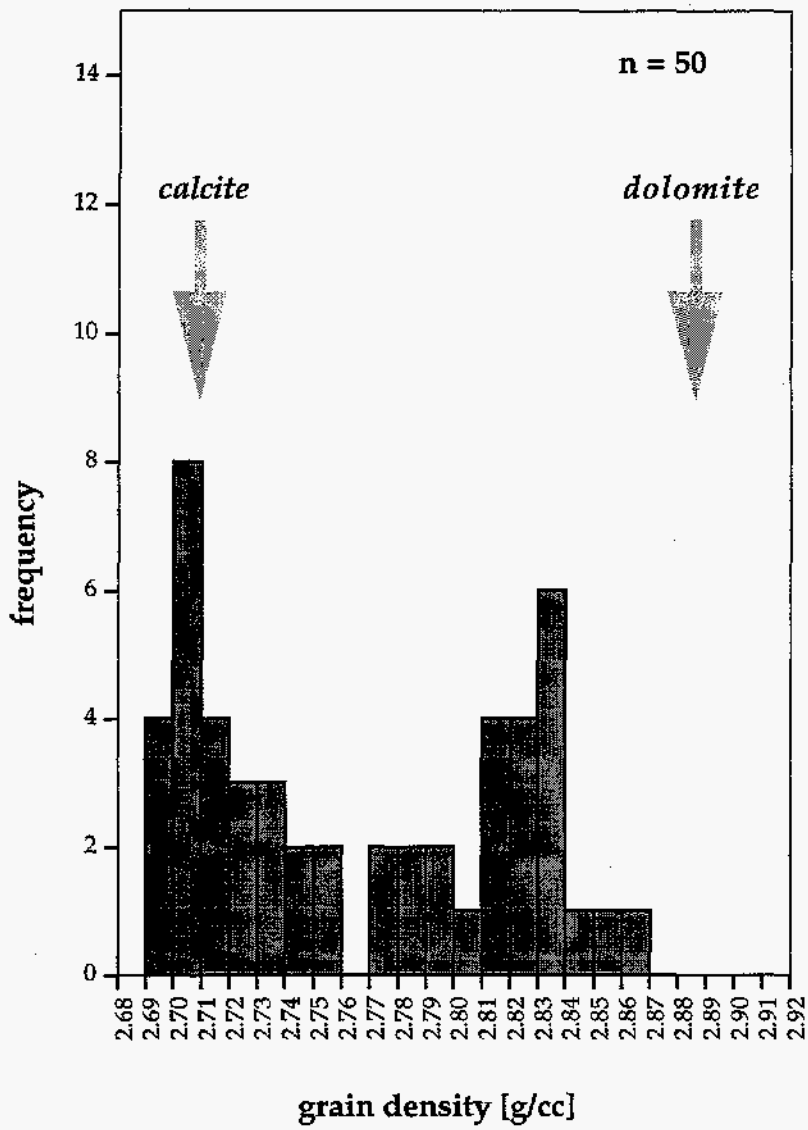

Fig. 7: Frequency distribution of grain-density data for carbonate rocks of the Maynardville Limestone and Copper Ridge Dolomite (Bear Creek Valley, ORR) based on helium porosimetry. Arrows indicate the grain densities of the minerals calcite and dolomite as provided by Olhoeft and Johnson (1989).

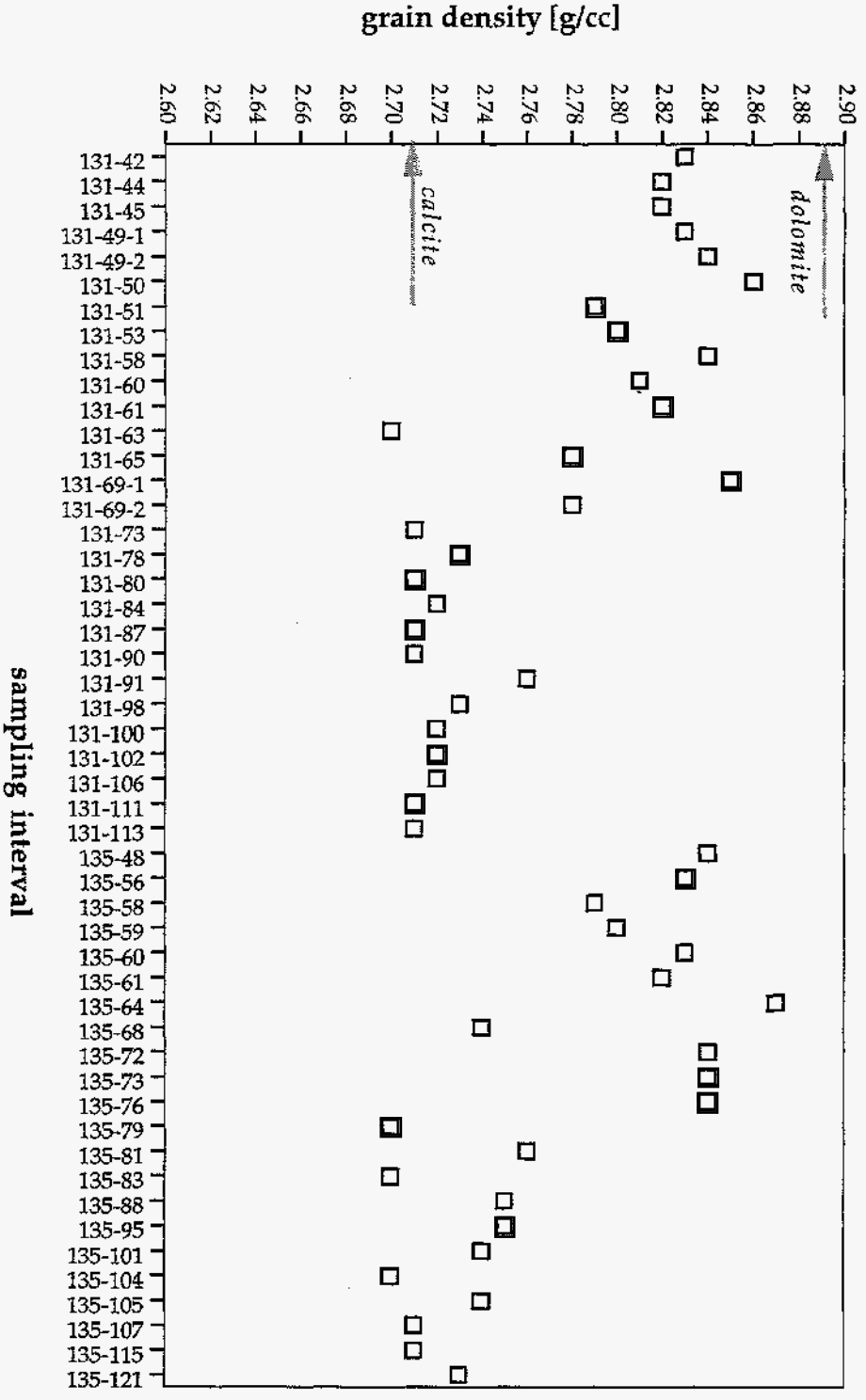

Fig. 8: Scatter plot of grain-density data for carbonate rocks of the Maynardville Limestone and Copper Ridge Dolomite (Bear Creek Valley, ORR) based on helium porosimetry. Arrows indicate the grain densities of the minerals calcite and dolomite as provided by Olhoeft and Johnson (1989).

Maynardville Limestone from corehole GW-135 appear to be higher, though only minimally, than comparable data from corehole GW-131.

Comparison and Evaluation of Density Data. The division of grain-density data into two distinct populations (Fig. 7) clearly distinguishes limestone from dolostone specimens. Limestone specimen grain-densities cluster around the mode centered on the 2.71 $g \cdot cm^{-3}$ class. Dolostone specimen grain-densities cluster around the mode centered on the 2.83 $g \cdot cm^{-3}$ class. The shift of the measured values to the left of the dolomite-mineral density (Fig. 7) probably reflects that dolostone of the Copper Ridge Dolomite and Maynardville Limestone also includes minerals of a grain density <2.88 $g \cdot cm^{-3}$. The most likely explanation is a mix of dominant dolomite with subordinate calcite. In the scatter diagram (Fig. 8) limestone specimens clearly cluster tightly along the "calcite line," whereas dolostone specimens display distinctly higher grain-density values with a larger scatter. The larger scatter might reflect the more complicated diagenetic history of the dolostone specimens which includes dolomitization and dedolomitization and their attendant changes to the mineralogy of the protolith.

The distribution of bulk densities is more complicated and the distinction between dolostone and limestone specimens is less clear (Fig. 5), because bulk densities also incorporate the interconnected and isolated void space contained within the analyzed specimens. For the majority of the data, limestone and dolostone specimens fall within their fields of reported bulk-density ranges as summarized by Olhoeft and Johnson (1989). There is a large area of overlap, however, in the reported data by Olhoeft and Johnson (1989) (Fig. 6), and this fact is also mirrored by the data from the ORR. Dolostone specimens with mineral matter of lower density or with higher porosity will plot within the dolostone/limestone overlap field, or even within the limestone field. The latter is drastically exemplified by specimen 131-69-1, which displays the lowest bulk-density reading and plots within the limestone field (Fig. 6), but is in fact dolostone. The low bulk density is caused by the abundance of vuggy porosity. A comparison to measured grain density reveals that the solid mineral matter places the specimen clearly above the "calcite line" (Fig. 8).

Specimen grain-density data are generally higher than specimen bulk-density data, because grain densities report the density of the solid material exclusively. There are, however, instances where both density types are identical or nearly identical for the same sampling interval (Appendix II). This might be explained by the absence or near absence of open void space (connected or isolated) in these specimens. This

interpretation is supported when examining the effective porosity data (i. e., interconnected void space) for the same sampling intervals, which display effective porosity values <0.7% (and generally much smaller; see below). Matching grain and bulk-density values (in concert with low effective porosity values) are the rule for limestone specimens, which is clearly displayed by Maynardville Limestone zones 1 through 5 from coreholes GW-131 and GW-135 (Figs. 9 and 10). Furthermore, some dolostone specimens from Maynardville Limestone zone 6 and from the Copper Ridge Dolomite show the same pattern. Most analyzed dolostone specimens, however, display more deviating bulk-density and grain-density values (commensurate with higher effective porosity values) (Figs. 9 and 10). Comparison of the density data by itself supports the petrographic observation by Goldstrand (1995) that all (or nearly all) primary porosity was occluded, and that the present "matrix porosity" is secondary in origin and most pronounced in dolostone, most likely related to dedolomitization.

Specimen Density with Depth. For both coreholes, density data show an overall decrease in value with depth and an overall decrease in scatter (Figs. 9 and 10) reflecting the increase in limestone and the decrease in dolostone with depth. As already pointed out, the discrepancy between bulk-density and grain-density values for specimens from the same sampling interval decreases with depth, with limestone specimens showing identical/nearly identical density values and dolostone specimens showing predominantly larger deviations between bulk-density and grain-density values (Figs. 9 and 10).

Comparison to Goldstrand's Bulk Density-Data. A comparison of bulk densities based on the Archimedes mercury immersion-technique (this study) and based on a water-displacement technique (Goldstrand et al., 1995) is shown in Figure 11. The data of Goldstrand et al. (1995) are exclusively from the Maynardville Limestone, and range from a minimum of 2.31 $g \cdot cm^{-3}$ to a maximum of 2.95 $g \cdot cm^{-3}$ with an arithmetic mean of 2.66 ($\pm$0.15) $g \cdot cm^{-3}$. Equivalent data for the Maynardville Limestone based on the Archimedes mercury immersion-technique display a much smaller range and a tighter cluster than the data reported by Goldstrand et al. (1995). The significant discrepancy of the two data sets is most likely caused by the inaccuracy of the water-displacement technique in determining bulk volume (as the basis for calculating bulk density) when compared to the Archimedes mercury immersion-technique. The Archimedes mercury immersion-technique is considered to be the most accurate and most reproducible method available (Thomas and Pugh, 1989).

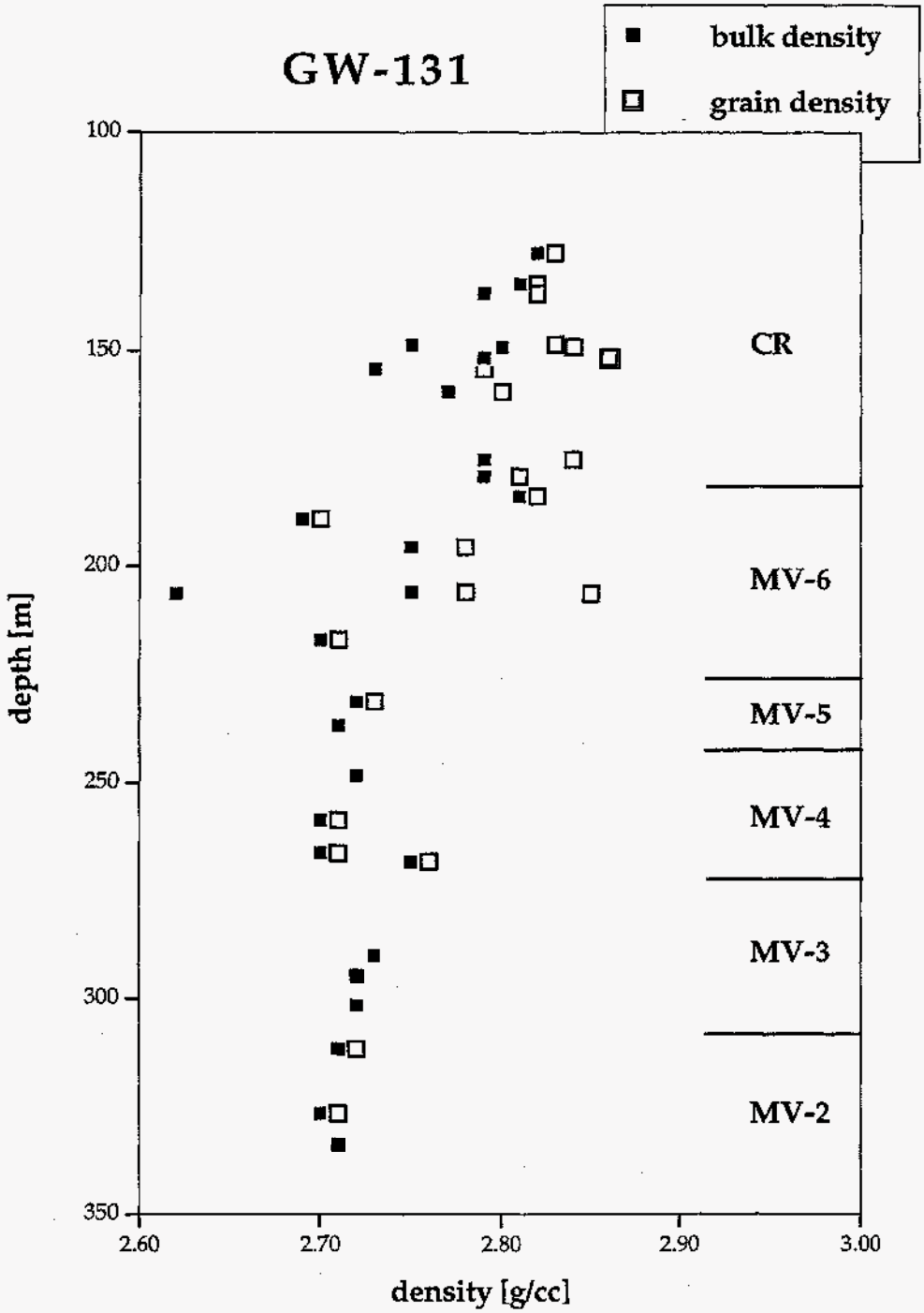

Fig. 9: Change of specimen bulk- and grain-density with depth below ground surface for carbonate rocks of the Copper Ridge Dolomite (CR) and Maynardville Limestone (MV, zones 1 through 6) (Bear Creek Valley, ORR) within corehole GW-131. (Note: if there is a correspondence in value of the two densities for the same depth, only the bulk-density data point is plotted.)

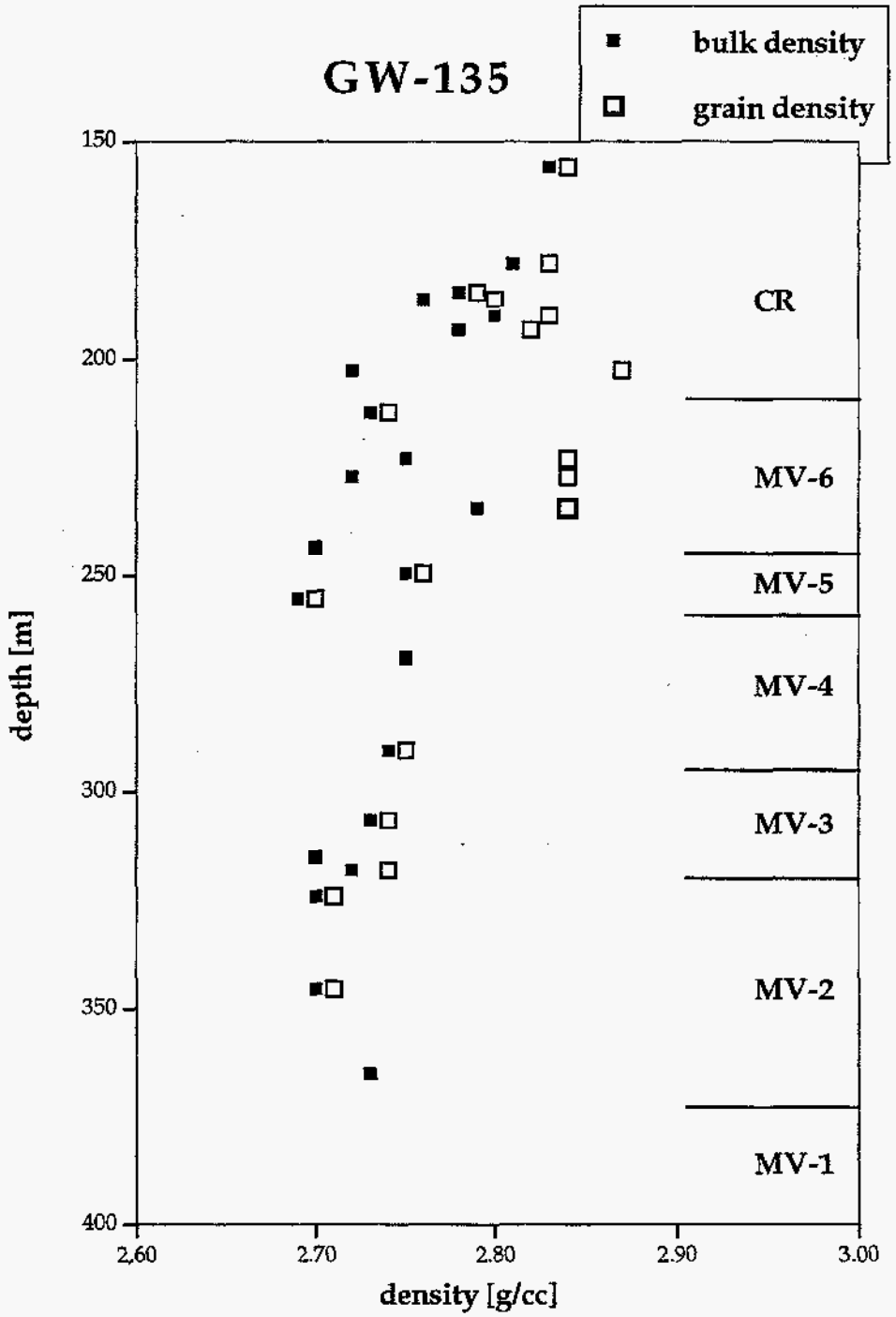

Fig. 10: Change of specimen bulk- and grain-density with depth below ground surface for carbonate rocks of the Copper Ridge Dolomite (CR) and Maynardville Limestone (MV, zones 1 through 6) (Bear Creek Valley, ORR) within corehole GW-135. (Note: if there is a correspondence in value of the two densities for the same depth, only the bulk-density data point is plotted.)

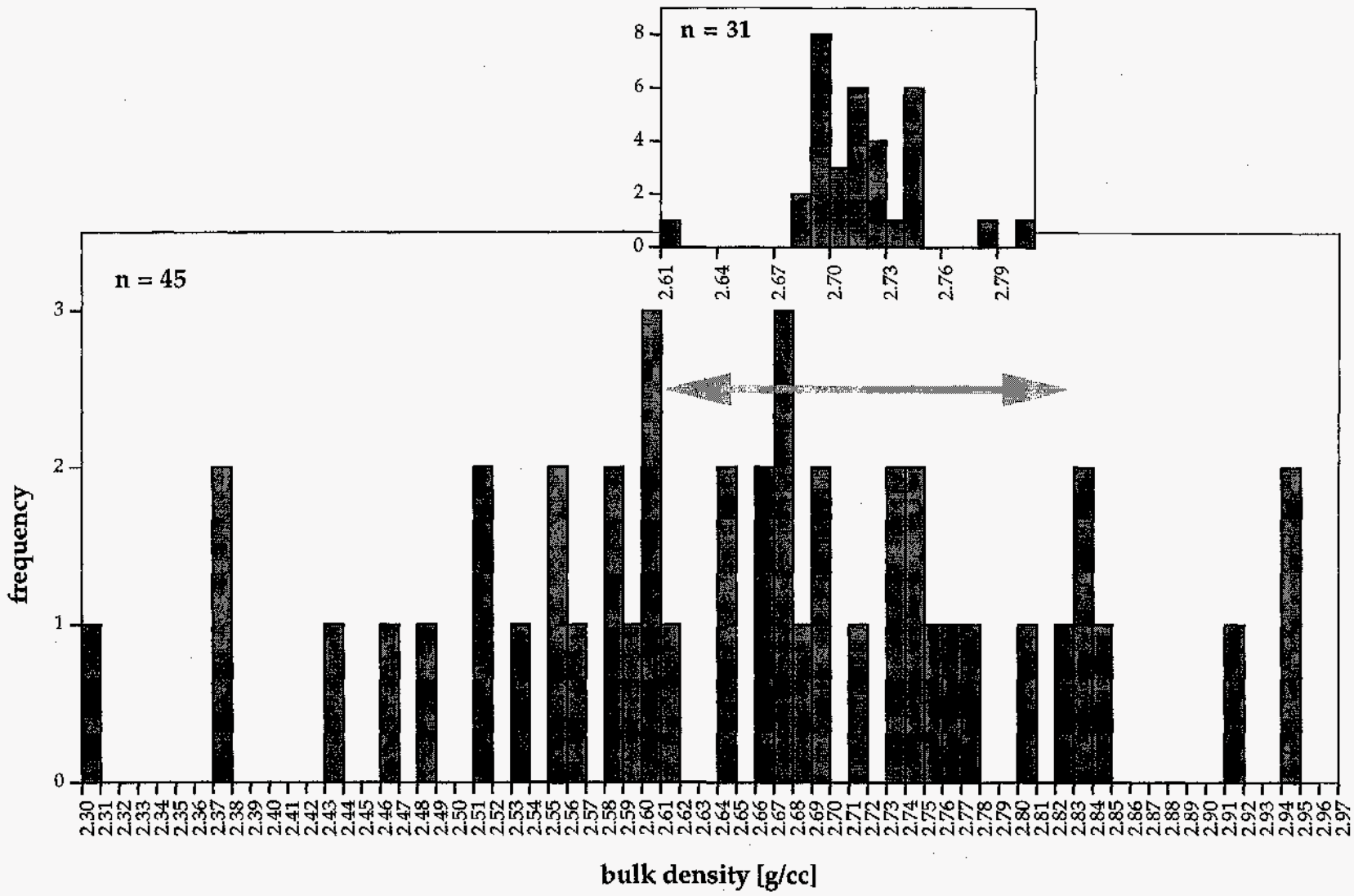

Fig. 11: Frequency distribution of bulk-density data for carbonate rock of the Maynardville Limestone (Bear Creek Valley, ORR) based on the water-displacement method as reported by Goldstrand et al. (1995). The arrow outlines the range of bulk-density data for the Maynardville Limestone *and* Copper Ridge Dolomite based on mercury immersion-technique (this study). The histogram insert displays the frequency distribution of these mercury-immersion data only for the Maynardville Limestone for a direct comparison of the two data sets (please note the difference in frequency scale between insert and main figure).

Effective Porosity Data

Effective porosity data from the Maynardville Limestone and from the Copper Ridge Dolomite from coreholes GW-131 and GW-135 are summarized in Appendix IV (based on helium porosimetry) and Appendix V (based on the immersion-saturation method). Calculated statistical measures are tabulated in Appendix VI (note that some statistical measures are based on a small number of samples).

Helium Porosimetry. The values of effective porosity based on helium porosimetry range from a maximum of 8.13% to a minimum of 0.06%. Based on all data, the arithmetic mean is 1.04 (±1.47%). The vast majority of the values are <1.8% with a prominent mode centered on the 0.3% class (Fig. 12). Because of some effective porosity values larger/considerably larger than 1.8%, the scatter within the data set is noteworthy (Fig. 13). Overall, data from GW-131 and GW-135 are very similar for the separate stratigraphic units. The highest average effective porosity values together with the largest standard deviation are encountered within zone 6 of the Maynardville Limestone; below zone 6 average effective porosity values decrease abruptly and are <<1.0%. There is also a decrease in average effective porosity from zone 5 to zone 2 of the Maynardville Limestone in corehole GW-135, whereas corehole GW-131 does not display such a trend.

Immersion-Saturation Method. Based on all data, the arithmetic mean of effective porosity values as determined with the immersion-saturation method is 1.00 (±1.0%), which is virtually identical with the helium-porosimetry data. The values range from a maximum of 4.52% to a minimum of 0.14%. The great majority of the values is <2.0%, with a distinct mode centered on the 0.3 class (Fig. 14). The scatter within the data set again is noticeable (Fig. 15). Effective porosity data are very similar when equivalent stratigraphic zones from coreholes GW-131 and GW-135 are compared. Average effective porosity values are highest in the Copper Ridge Dolomite, then decrease into zone 6 of the Maynardville Limestone, and then decrease sharply into zones 5 through 2 of the Maynardville Limestone. There is no clear trend of decreasing average effective porosity discernible for zones 5 through 2 from both coreholes; average effective porosity values, however, are consistently <<1.0% throughout this interval.

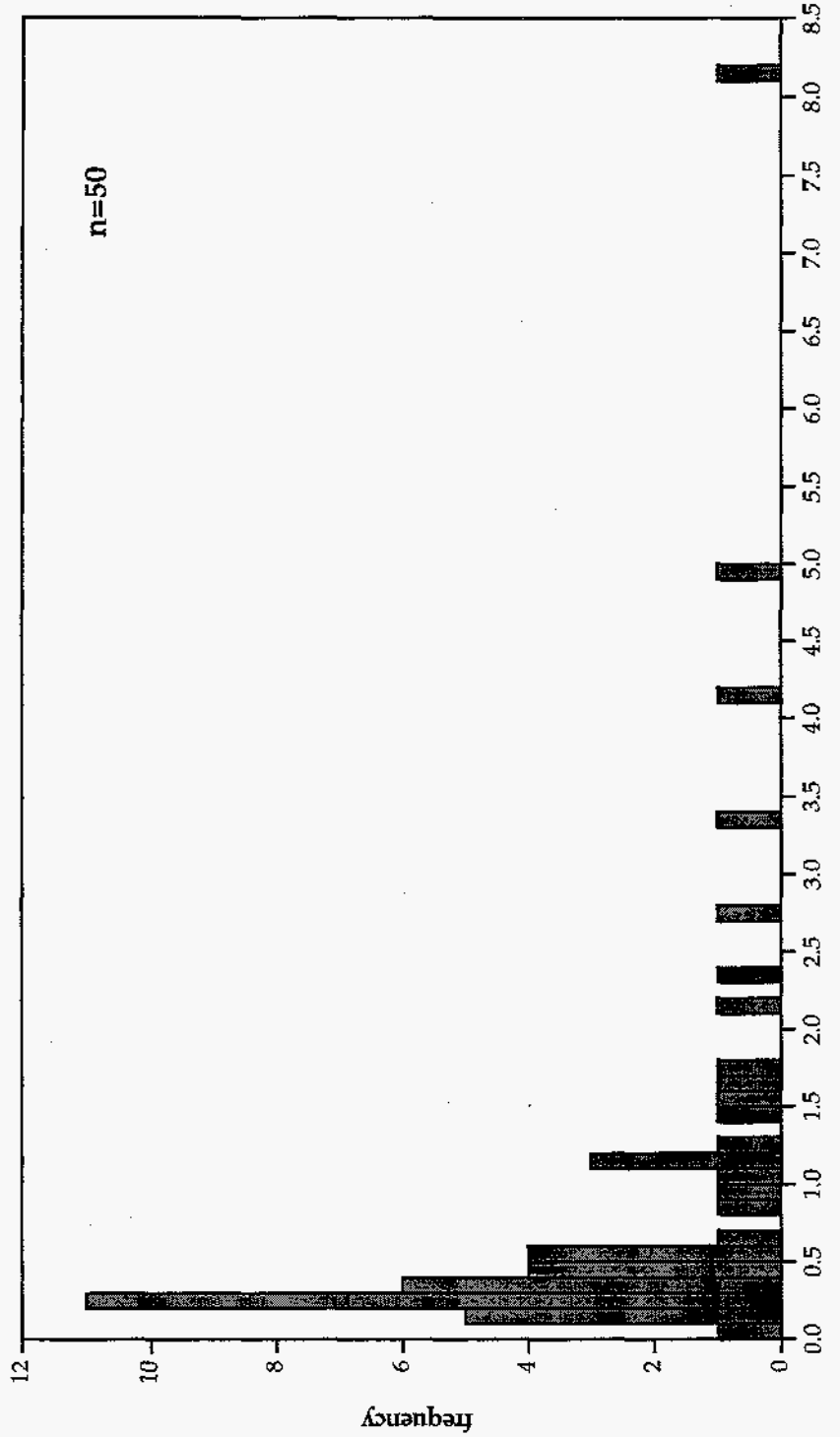

Fig. 12: Frequency distribution of effective porosity values based on helium porosimetry.

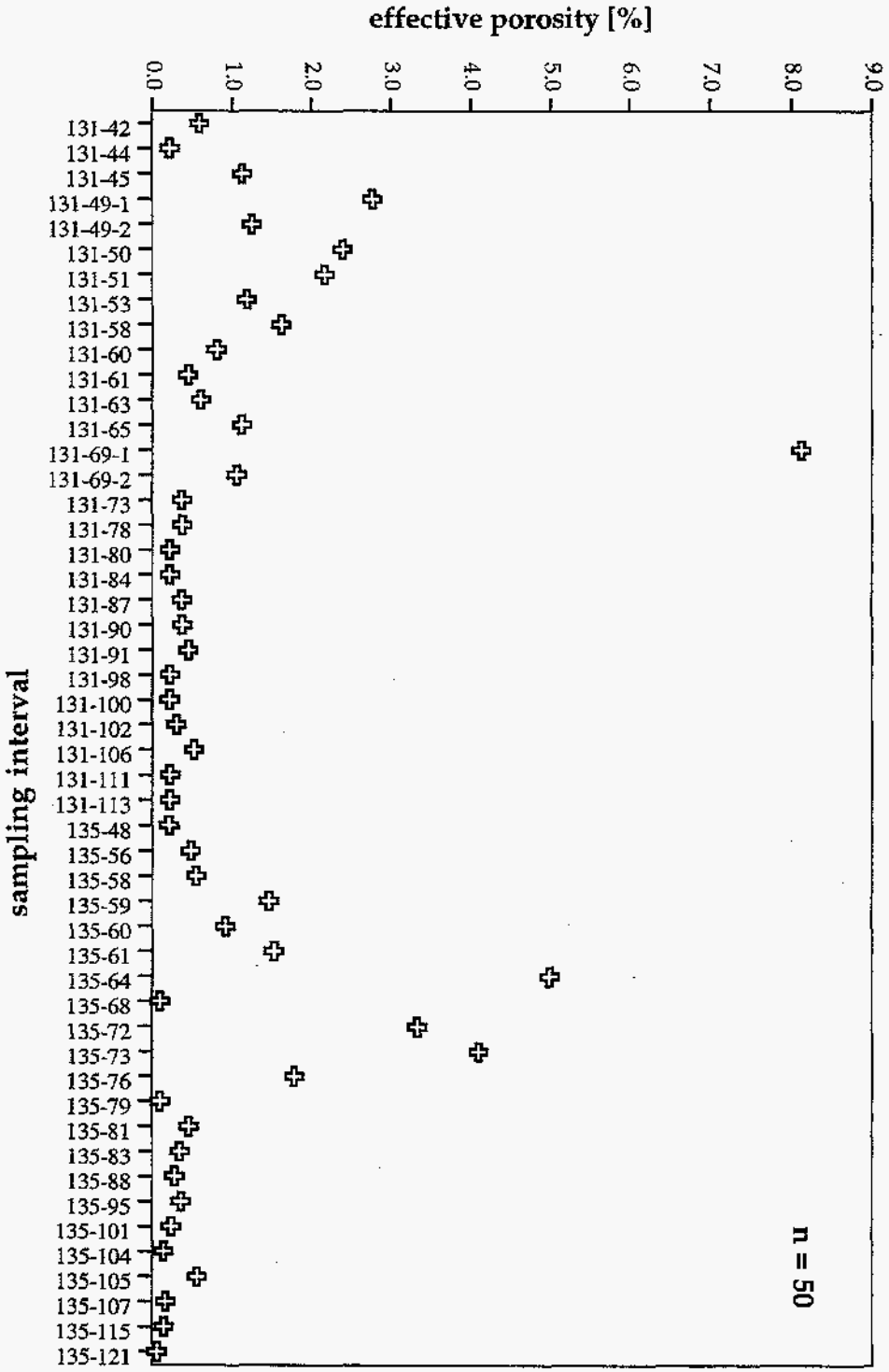
effective porosity [%]
0.0
1.0
2.0
3.0
4.0
5.0
6.0
7.0
8.0
9.0
sampling interval
131-42
131-44
131-45
131-49-1
131-49-2
131-50
131-51
131-53
131-58
131-60
131-61
131-63
131-65
131-69-1
131-69-2
131-73
131-78
131-80
131-84
131-87
131-90
131-91
131-98
131-100
131-102
131-106
131-111
131-113
135-48
135-56
135-58
135-59
135-60
135-61
135-64
135-68
135-72
135-73
135-76
135-79
135-81
135-83
135-88
135-95
135-101
135-104
135-105
135-107
135-115
135-121
n = 50

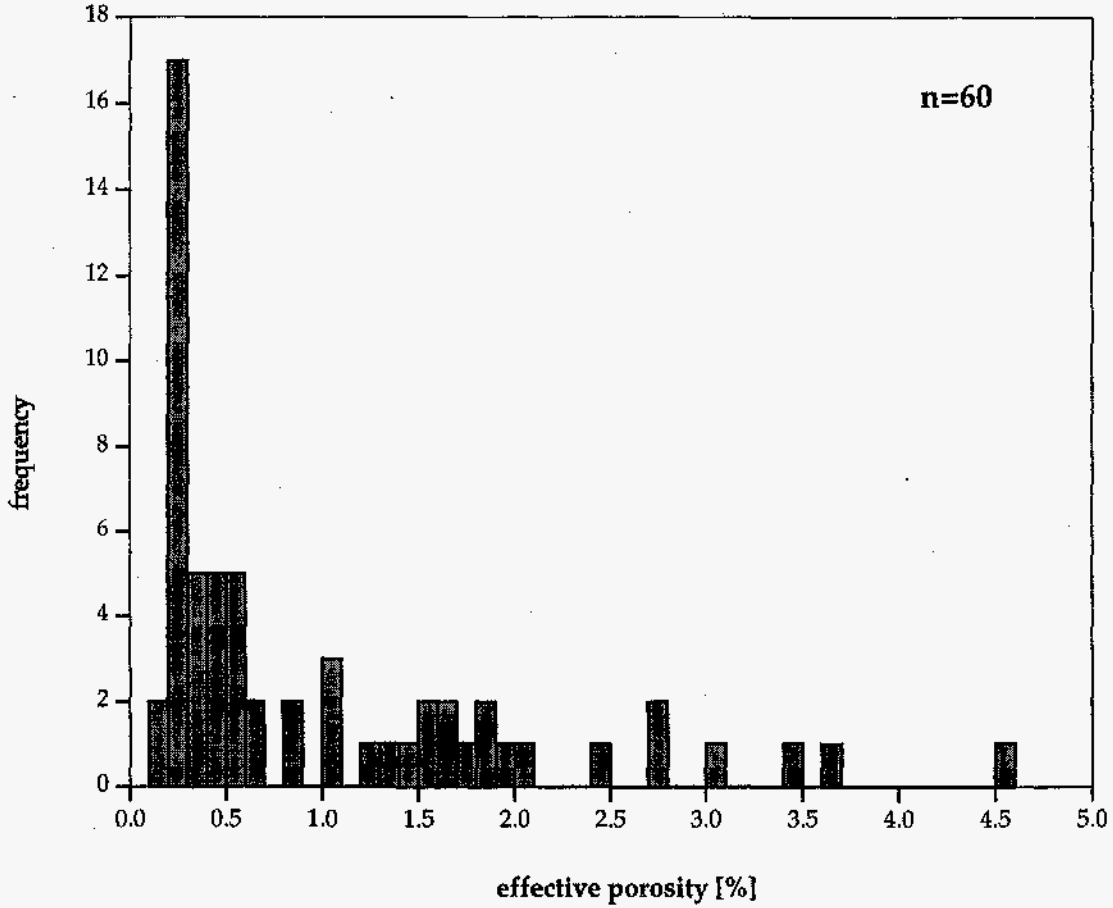

Fig. 14: Frequency distribution of effective porosity values based on the immersion-saturation method.

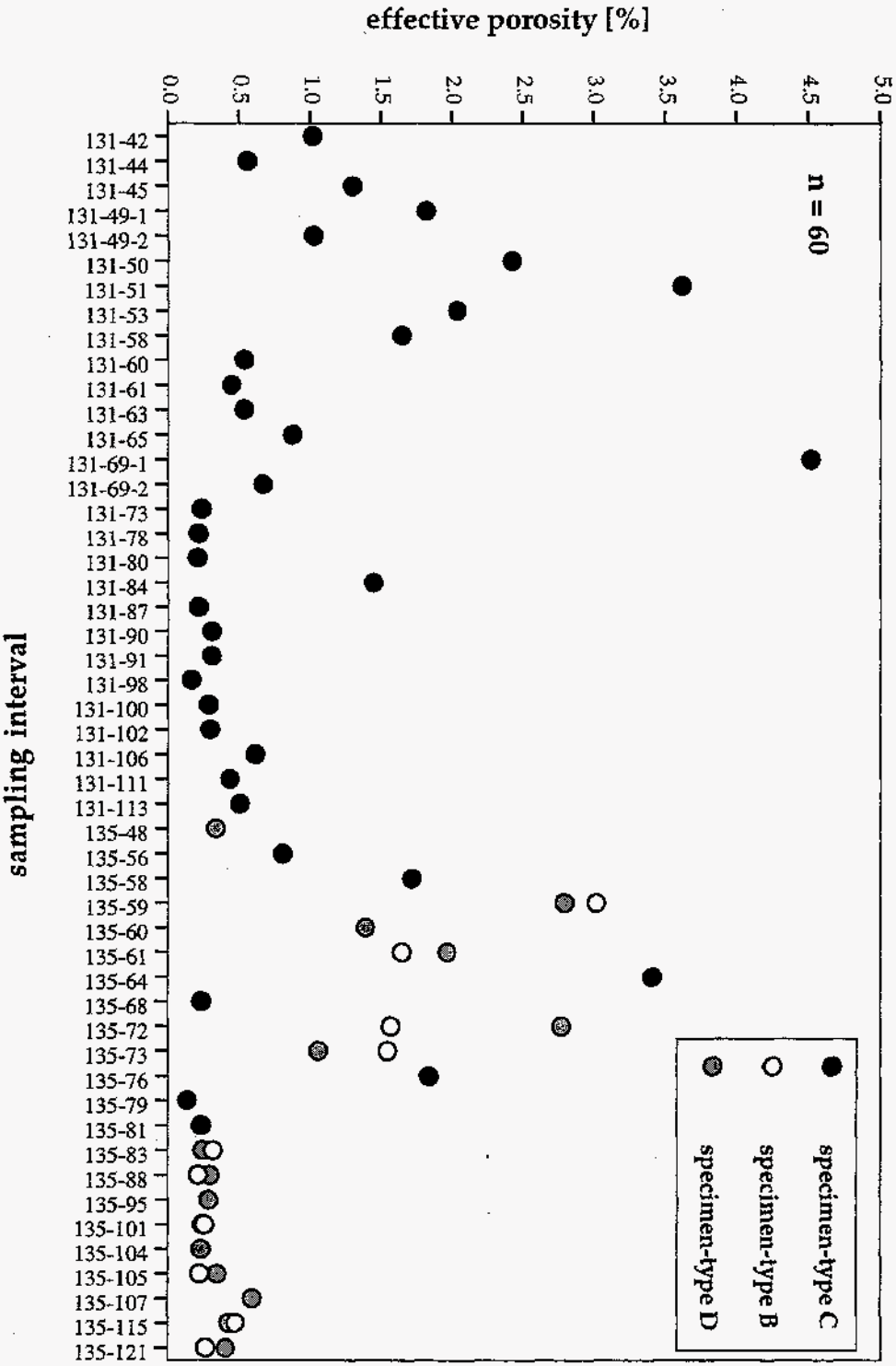
effective porosity [%]
0.0
0.5
1.0
1.5
2.0
2.5
3.0
3.5
4.0
4.5
5.0
n = 60
sampling interval
131-42
131-44
131-45
131-49-1
131-49-2
131-50
131-51
131-53
131-58
131-60
131-61
131-63
131-65
131-69-1
131-69-2
131-73
131-78
131-80
131-84
131-87
131-90
131-91
131-98
131-100
131-102
131-106
131-111
131-113
135-48
135-56
135-58
135-59
135-60
135-61
135-64
135-68
135-72
135-73
135-76
135-79
135-81
135-83
135-88
135-95
135-101
135-104
135-105
135-107
135-115
135-121
specimen-type C
specimen-type B
specimen-type D

Comparison and Evaluation of Effective Porosity Data. The distribution of helium-porosimetry and immersion-saturation data is very similar. Both histograms (Figs. 12, 14) display a pronounced mode centered on the 0.3% class and are distinctly skewed to the right (with a long tail of values stretching toward larger effective porosity values). Average effective porosity values based on the different methods are also virtually identical (Appendix VI).

A crossplot of effective porosity based on helium porosimetry versus effective porosity based on the immersion-saturation method for specimens from the same sampling interval (Fig. 16) reveals that the majority of data points show a good correspondence and plot at or close to the 1-to-1 line. This indicates that for most cases the results from the two petrophysical techniques were identical or nearly identical. There are, however, deviations from this ideal situation, with both examples of deviating higher helium-porosity values and immersion-saturation porosity values. Figures 17 and 18 show that an excellent match between helium-porosimetry and immersion-saturation data for the same sampling interval are the rule for limestone specimens (Maynardville zones 2 through 5, also in zone 6). Furthermore, many dolostone specimens from the Copper Ridge Dolomite and the Maynardville Limestone zone 6 show excellent to good correspondence, but there are also examples with a significant deviation between values based on the different measurement techniques.

Effective porosity data based on helium porosimetry and the immersion-saturation method both display low values and a small scatter for limestone specimens (131-73 through 131-113; 135-68, 135-79 through 135-121; Figs. 13, 15). Dolostone specimens, in contrast, show a much wider scatter in effective porosity values. These observations again indicate the severe effect of cementation and the loss of interconnected pore space for limestone specimens (see also Goldstrand, 1995; Goldstrand et al., 1995). Later diagenetic events, such as dolomitization and dedolomitization, is responsible for the higher and more varied effective porosity values for dolostone specimens. Most of the higher effective porosity values are associated with specimens displaying vuggy porosity (131-50, 131-51, 131-69-1; 135-72, 135-73, 135-76). These high porosity values indicate a good interconnectivity between the pore types which was probably caused by dedolomitization (Goldstrand, 1995). However, there are examples of specimens with vuggy porosity which show effective porosity below or at 1% (131-45,131-80, 131-84; 135-58, 135-83). These examples highlight that vuggy porosity might be present but poorly interconnected, giving rise to low effective porosity values.

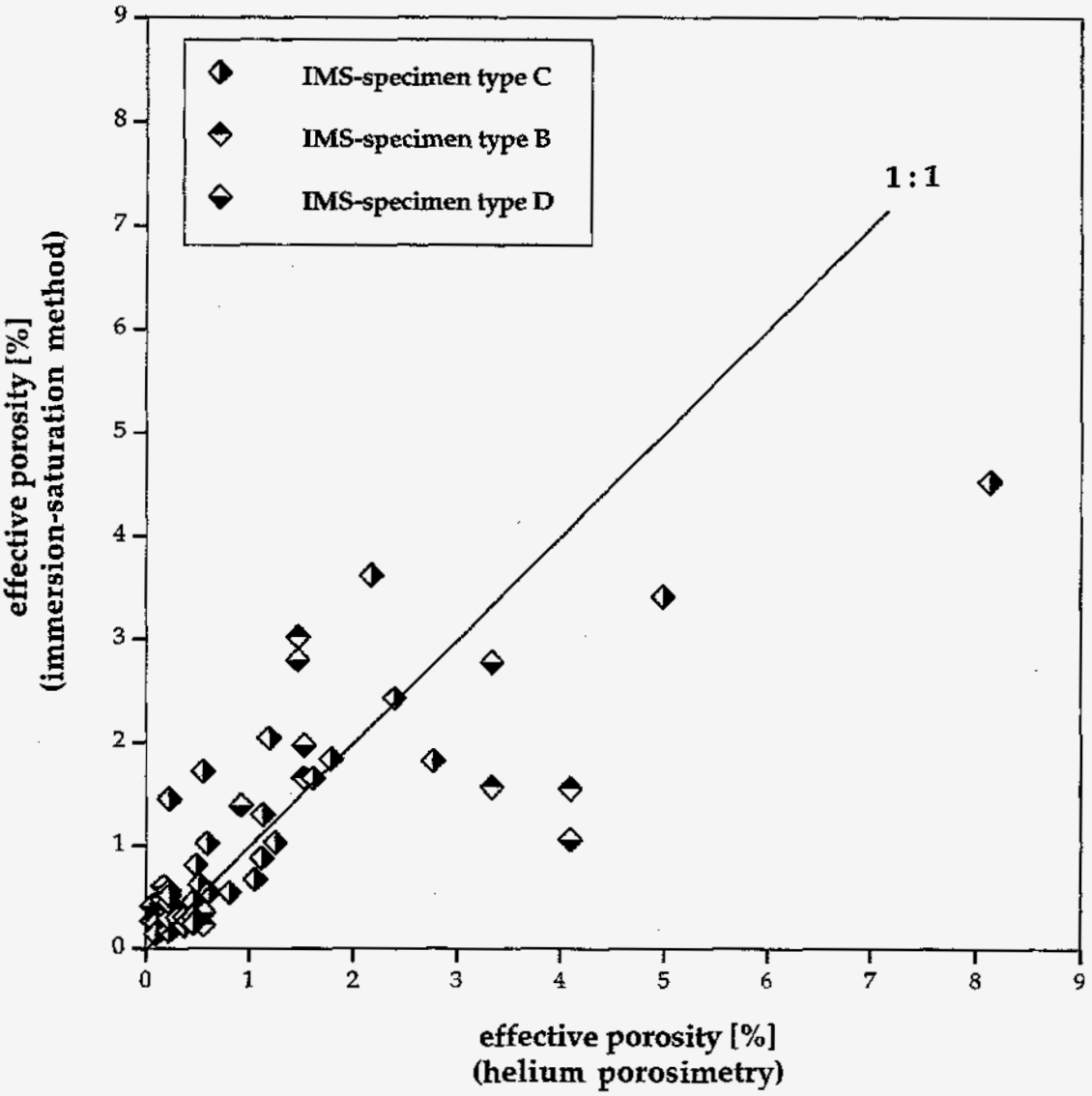

Fig. 16: Diagram plotting effective porosity based on the immersion-saturation method against effective porosity based on helium porosimetry. Specimens are limestone and dolostone from the Copper Ridge Dolomite and Maynardville Limestone (Bear Creek Valley, ORR). The different specimen types used for the immersion-saturation method are core plugs (-B), disks (-C), and box shapes (-D).

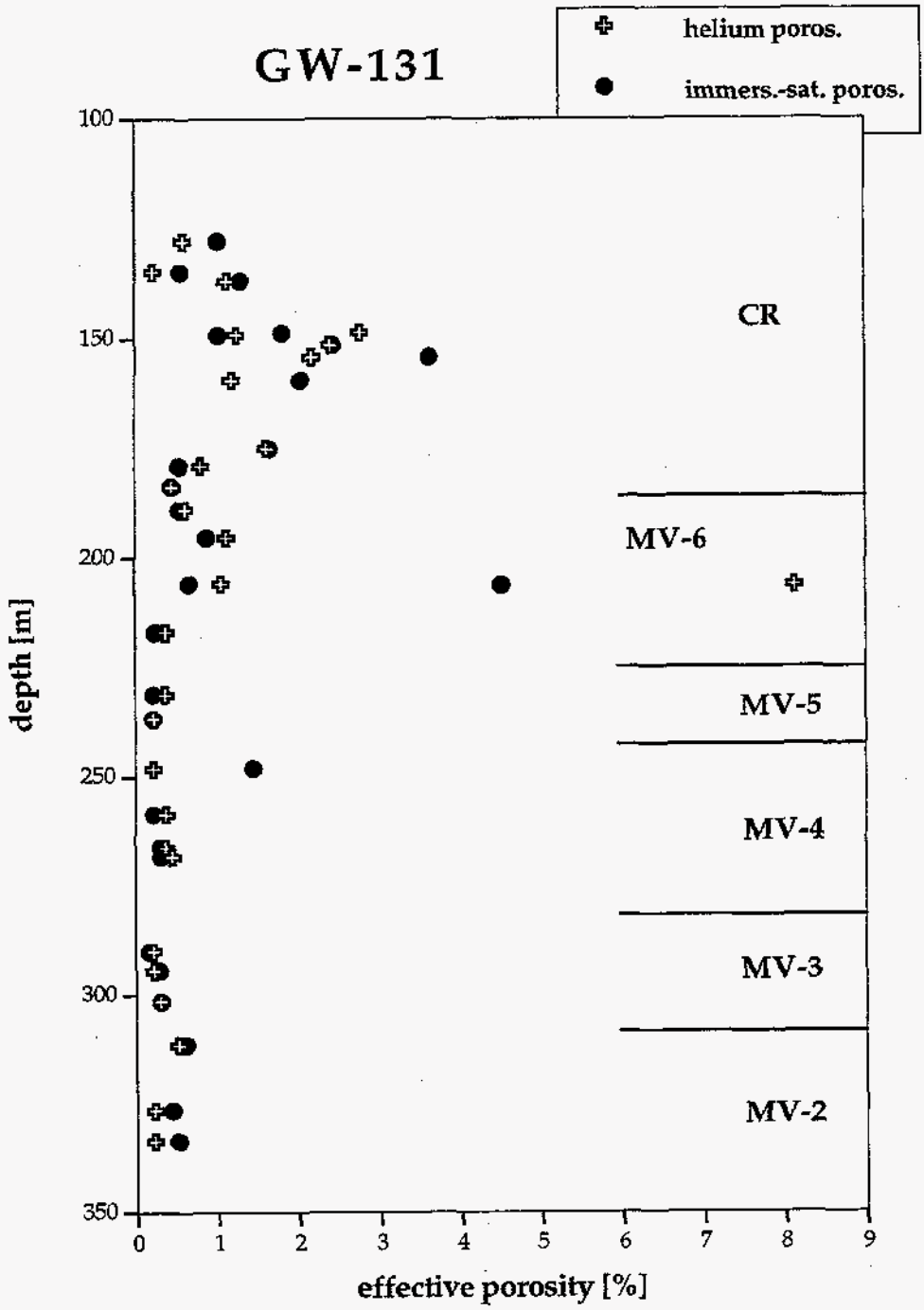

Fig. 17: Change of effective porosity with depth below ground surface for carbonate rocks of the Copper Ridge Dolomite (CR) and Maynardville Limestone (MV, zones 1 through 6) (Bear Creek Valley, ORR) within corehole GW-131.

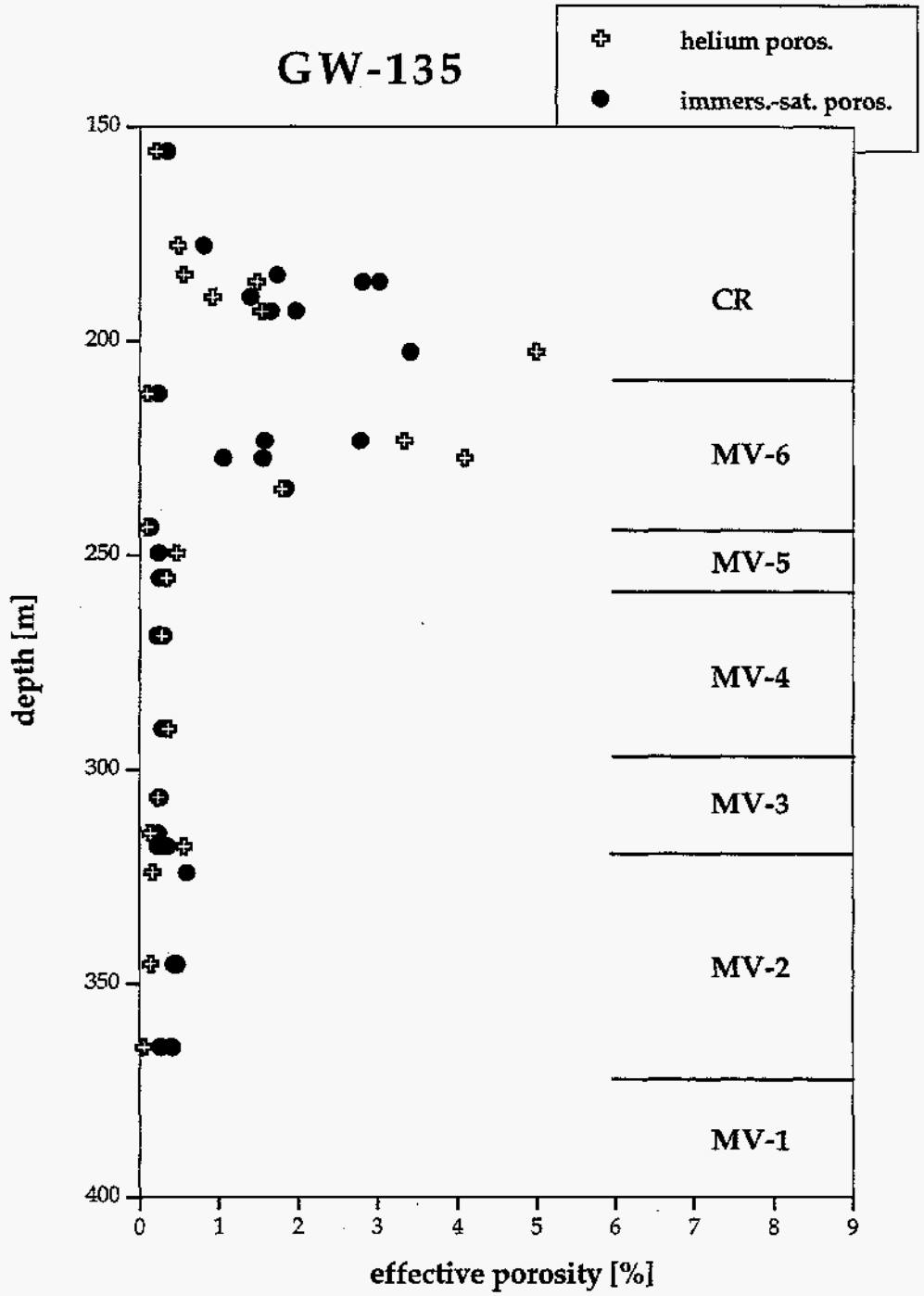

Fig. 18: Change of effective porosity with depth below ground surface for carbonate rocks of the Copper Ridge Dolomite (CR) and Maynardville Limestone (MV, zones 1 through 6) (Bear Creek Valley, ORR) within corehole GW-135.

Specimens of different weight (and different volume) were available from some of the sampling intervals from corehole GW-135 and were analyzed with the immersion-saturation method. Core-plug specimens (suffix -B) were a little more than twice the weight than box-shaped specimens (suffix -D). Overall, the effective porosity values compare very well (Appendix V; Fig. 15), especially for limestone specimens. This observation indicates that the different weights/volumes did not influence the effective porosity results, at least not at the studied volumes. The differences are somewhat larger for most of the analyzed dolostone specimens. This observation might be explained with the much larger porosity heterogeneity for dolostone specimens from the Copper Ridge Dolomite and Maynardville Limestone when compared with limestone specimens, rather than indicating the influence of differing volumes analyzed.

Comparison to Goldstrand's Porosity Data. Effective porosity data based on helium porosimetry, the immersion-saturation method and the water-immersion method (as used by Goldstrand et al., 1995) were available for nineteen sampling intervals from corehole GW-135 (Appendix VII). This enables a direct comparison of effective porosity values as reported in this study and as reported in Goldstrand et al. (1995) (Fig. 19).

For limestone specimens (135-68, 135-79 through 135-121) effective porosity values are predominantly low (<1%). Furthermore, the match between the values obtained with the different methods is good to excellent, with the exception of sampling intervals 135-79, 135-83 and 135-95 (Fig. 19). These intervals display matching effective porosity values based on helium porosimetry and the immersion-saturation method, with a significant deviation toward higher values based on the water-immersion method as used by Goldstrand et al. (1995). Sampling interval 135-83 (Goldstrand's effective porosity is 7.7 times higher) displays vuggy porosity and the deviating effective porosity values, therefore, might tentatively be explained with the porosity heterogeneity of that sampling interval. Sampling intervals 135-79 (Goldstrand's effective porosity is 10.0 times higher) and 135-95 (Goldstrand's effective porosity is 2.4 times higher) are not from vuggy limestone intervals, and the deviation of the results by Goldstrand et al. (1995) might point to a problem with the chosen analysis technique.

For dolostone specimens (135-58 through 135-64, and 135-72 through 135-76) a much greater degree of scatter between the effective porosity values based on the different analysis techniques is apparent (Fig. 19). This probably reflects the influence of secondary porosity which dominates the porosity within the analyzed intervals of the

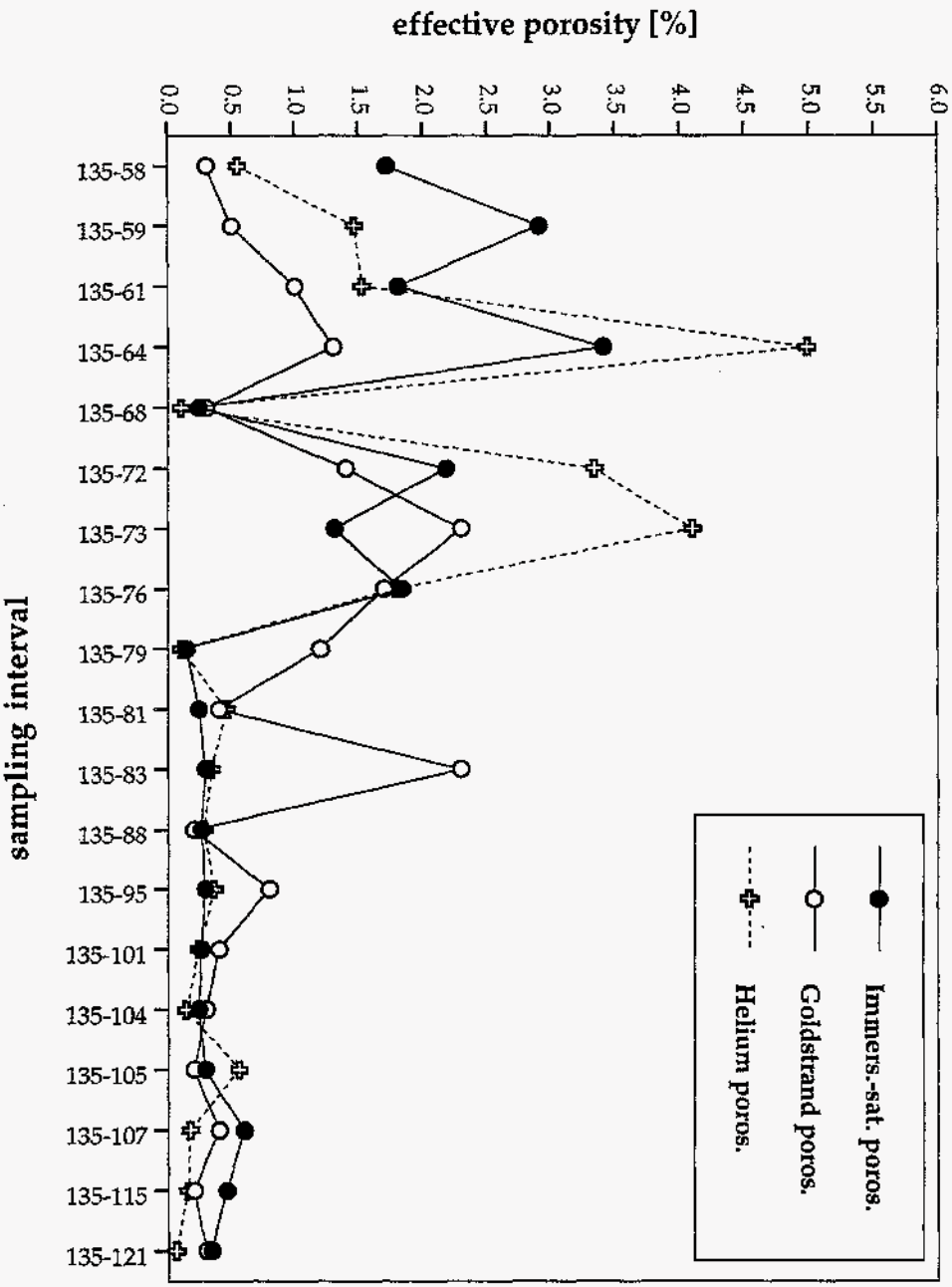
effective porosity [%]
0.0
0.5
1.0
1.5
2.0
2.5
3.0
3.5
4.0
4.5
5.0
5.5
6.0
sampling interval
135-58
135-59
135-61
135-64
135-68
135-72
135-73
135-76
135-79
135-81
135-83
135-88
135-95
135-101
135-104
135-105
135-107
135-115
135-121
Immers.-sat. poros.
Goldstrand poros.
Helium poros.

Copper Ridge Dolomite and Maynardville Limestone (Goldstrand et al., 1995). Although direct matches between values are rare, the overall trend of effective porosity values based on the different methods remains similar (Fig. 19). In general, helium porosimetry values or values based on the immersion-saturation method are the highest, with Goldstrand's effective porosity data consistently displaying the lowest values (except for 135-73). The consistently low values based on the methodology of Golstrand et al. (1995) are most likely related to insufficient saturation time (a possible source of error already pointed out by Goldstrand et al., 1995) and to an underestimation of bulk-density values. These two sources of error have their most significant effect on the effective porosity results for dolostone specimens, which possess more interconnected pore space; they do not appear to have the same influence on the effective porosity results of limestone specimens, which display far less interconnected pore space. The higher effective porosity in dolostone specimens also suggests that insufficient saturation with water and an underestimation of the saturated specimen weight is the probable main reason for the low effective porosity values based on Goldstrand's methodology.

Effective Porosities with Depth. For both coreholes, effective porosity values based on helium porosimetry and the immersion-saturation method, together with the scatter in the data, decrease with depth within corehole GW-131 and GW-135 (Figs. 17, 18). As mentioned previously, there is a dramatic drop in effective porosity values and scatter from the middle part of zone 6 of the Maynardville Limestone to the base of zone 6 /top of zone 5 (Figs. 17, 18). Effective porosity values are uniformly low from zone 5 through zone 2 of the Maynardville Limestone. The distribution of helium-porosimetry and immersion-saturation effective porosity data with depth also exhibit the predominantly good to excellent fit for specimens from the same sampling interval. The highest effective porosity values are encountered in the middle to lower part of the analyzed range of the Copper Ridge Dolomite and within the middle part of zone 6 of the Maynardville Limestone. The trends of effective porosity and scatter with depth reflect the increase in limestone at the expense of dolostone with depth. The distribution of effective porosity values with depth and stratigraphy corresponds to the observations of Goldstrand et al. (1995). The trends, furthermore, parallel trends observed already from specimen-density data.

CONCLUSIONS

1. Specimens of carbonate rock (limestone and dolostone) from sampling intervals of the Copper Ridge Dolomite and Maynardville Limestone (coreholes GW-131 and GW-135, Bear Creek Valley) were analyzed with helium porosimetry and the immersion-saturation method. These techniques provide state-of-the-art petrophysical data on effective porosity and specimen densities (Table 1).

2. Specimen grain-density data display a bimodal distribution and range from 2.70 $g \cdot cm^{-3}$ to 2.87 $g \cdot cm^{-3}$. The two modes clearly reflect the mineralogy of the analyzed specimens, that is calcite for limestone and dolomite + calcite for dolostone. Specimen bulk-density data range from 2.62 $g \cdot cm^{-3}$ to 2.83 $g \cdot cm^{-3}$. In comparison, the range of bulk-density data reported by Goldstrand et al. (1995) is much larger. This deviation can be explained with the inherent inaccuracy of the water-displacement technique (as used by Goldstrand et al., 1995) when compared to the Archimedes mercury immersion-technique (this study).

3. Effective porosity values determined with helium porosimetry range from 0.06% to 8.13%, whereas the immersion-saturation technique yielded values from 0.14% to 4.52%. For both petrophysical methods, the vast majority of effective porosity values is <2% with a distinct mode centered on the 0.3% class. Effective porosities <1% or <<1% are the rule for limestone specimens and reflect the pervasive cementation; dolostone specimens can display such low values, but commonly exhibit values >1% or >>1% reflecting the widespread development of secondary porosity (dedolomitization; see Goldstrand et al., 1995). In general, the match between helium-porosimetry and immersion-saturation data for the same sampling interval is excellent to good. Specimens with vuggy porosity generally show higher effective porosity values, but there is a significant number of vuggy specimens with low effective porosity values indicating that the large pores are poorly connected.

4. The highest levels of effective porosity can be found within the middle to lower part of analyzed section of the Copper Ridge Dolomite and within the middle part of zone 6 of the Maynardville Limestone. There is a drastic drop in effective porosity from the middle part of zone 6 of the Maynardville Limestone to the subjacent parts of the Maynardville Limestone. This observation reflects the increase of ("tighter") limestone at the expense of dolostone with depth.

Table 1: Summary of petrophysical information on carbonate rock (limestone, dolostone) from the Maynardville Limestone and Copper Ridge Dolomite (Bear Creek Valley on the ORR). Asterick indicates that the value is an average of several values for this sampling interval.

core	samp. interv. [a]	depth [b]	strat. unit [c]	δHe [d] (g/cm^3)	δHg [e] (g/cm^3)	ϕHe [f] (%)	ϕIMS [g] (%)
GW-131	131-42	419' 2" (127.76 m)	CR	2.83	2.82	0.59	1.02
GW-131	131-44	442' 3" (134.80 m)	CR	2.82	2.81	0.22	0.56
GW-131	131-45	449' 4" (136.96 m)	CR	2.82	2.79	1.13	1.30
GW-131	131-49-1	487' 10" (148.69 m)	CR	2.83	2.75	2.77	1.82
GW-131	131-49-2	489' 7" (149.23 m)	CR	2.84	2.80	1.25	1.03
GW-131	131-50	497' 3" (151.56 m)	CR	2.86	2.79	2.40	2.43
GW-131	131-51	506' 2" (154.28 m)	CR	2.79	2.73	2.17	3.62
GW-131	131-53	523' 6" (159.56 m)	CR	2.80	2.77	1.19	2.04
GW-131	131-58	574' 8" (175.16 m)	CR	2.84	2.79	1.62	1.65
GW-131	131-60	587' 5" (179.05 m)	CR	2.81	2.79	0.81	0.54
GW-131	131-61	602' 9" (183.72 m)	MV (6)	2.82	2.81	0.45	0.45
GW-131	131-63	619' 10" (188.93 m)	MV (6)	2.70	2.69	0.61	0.54
GW-131	131-65	641' 3" (195.45 m)	MV (6)	2.78	2.75	1.12	0.88
GW-131	131-69-2	675' 7" (205.92 m)	MV (6)	2.78	2.75	1.06	0.67
GW-131	131-69-1	677' (206.35 m)	MV (6)	2.85	2.62	8.13	4.52
GW-131	131-73	712' (217.02 m)	MV (6)	2.71	2.70	0.37	0.24
GW-131	131-78	758' 9" (231.27 m)	MV (5)	2.73	2.72	0.37	0.22
GW-131	131-80	777' 2" (236.88 m)	MV (5)	2.71	2.71	0.22	0.21
GW-131	131-84	814' 6" (248.26 m)	MV (4)	2.72	2.72	0.22	1.45
GW-131	131-87	848' 6" (258.62 m)	MV (4)	2.71	2.70	0.37	0.22
GW-131	131-90	873' 7" (266.27 m)	MV (4)	2.71	2.70	0.37	0.31
GW-131	131-91	880' 2" (268.28 m)	MV (4)	2.76	2.75	0.45	0.31
GW-131	131-98	951' 7" (290.04 m)	MV (3)	2.73	2.73	0.22	0.17
GW-131	131-100	966' (294.44 m)	MV (3)	2.72	2.72	0.22	0.29
GW-131	131-102	989' 6" (301.60 m)	MV (3)	2.72	2.72	0.30	0.30
GW-131	131-106	1022' 2" (311.56 m)	MV (2)	2.72	2.71	0.52	0.62
GW-131	131-111	1071' 2" (326.49 m)	MV (2)	2.71	2.70	0.22	0.44
GW-131	131-113	1094' 6" (333.60 m)	MV (2)	2.71	2.71	0.22	0.51

Table 1: Continued

core	samp. interv. [a]	depth [b]	strat. unit [c]	δHe [d] (g/cm^3)	δHg [e] (g/cm^3)	ϕHe [f] (%)	ϕIMS [g] (%)
GW-135	135-48	511' 4" (155.85 m)	CR	2.84	2.83	0.21	0.34
GW-135	135-56	583' 3" (177.78 m)	CR	2.83	2.81	0.48	0.81
GW-135	135-58	605' 5" (184.53 m)	CR	2.79	2.78	0.55	1.72
GW-135	135-59	611' (186.23 m)	CR	2.80	2.76	1.47	2.91*
GW-135	135-60	622' 6" (189.74 m)	CR	2.83	2.80	0.92	1.39
GW-135	135-61	633' 6" (193.09 m)	CR	2.82	2.78	1.53	1.81*
GW-135	135-64	664' 4" (202.49 m)	CR	2.87	2.72	4.99	3.41
GW-135	135-68	696' 4" (212.24 m)	MV (6)	2.74	2.73	0.10	0.24
GW-135	135-72	732' (223.11 m)	MV (6)	2.84	2.75	3.34	2.18*
GW-135	135-73	745' 7" (227.25 m)	MV (6)	2.84	2.72	4.10	1.31*
GW-135	135-76	769' 2" (234.44 m)	MV (6)	2.84	2.79	1.79	1.84
GW-135	135-79	798' 9" (243.46 m)	MV (6)	2.70	2.70	0.10	0.14
GW-135	135-81	818' 8" (249.53 m)	MV (5)	2.76	2.75	0.46	0.24
GW-135	135-83	837' 11" (255.40 m)	MV (5)	2.70	2.69	0.34	0.29*
GW-135	135-88	882' 3" (268.91 m)	MV (4)	2.75	2.75	0.28	0.26*
GW-135	135-95	953' 2" (290.53 m)	MV (4)	2.75	2.74	0.36	0.29
GW-135	135-101	1005' 10" (306.58 m)	MV (3)	2.74	2.73	0.24	0.26*
GW-135	135-104	1033' 4" (314.96 m)	MV (3)	2.70	2.70	0.14	0.24
GW-135	135-105	1043' 4" (318.01 m)	MV (3)	2.74	2.72	0.56	0.29*
GW-135	135-107	1063' 3" (324.08 m)	MV (2)	2.71	2.70	0.17	0.60
GW-135	135-115	1133' 6" (345.49 m)	MV (2)	2.71	2.70	0.15	0.46*
GW-135	135-121	1197' 7" (365.02 m)	MV (2)	2.73	2.73	0.06	0.34*

a =sampling interval from which specimens were removed (Corehold number and box humber)
b =drill depth below ground surface
c =stratigraphic unit from which specimens were obtained, either Copper Ridge Dolomite (CR) or Maynardville Limestone (MV), with numbers in parentheses referring to the different zones of the Maynardville Limestone
d =specimen grain-density
e =specimen bulk-density
f =effective porosity based on helium porosimetry
g =effective porosity based on the immersion-saturation method

5. A direct comparison to the effective porosity data as determined with a water-immersion technique by Goldstrand et al. (1995) was possible for nineteen sampling intervals. The comparison revealed that the effective porosity of dolostone specimens (higher effective porosity) was systematically underestimated by Goldstrand et al. (1995). This observation can be related to the use of inaccurate bulk-density values and, probably more significant, to insufficient saturation times. For limestone specimens (lower effective porosity) effective porosity data of Goldstrand et al. (1995) match the helium-porosimetry and immersion-saturation data much better. There are, however, examples where higher/significantly higher values are reported based on Goldstrand's water-immersion technique.

REFERENCES

American Petroleum Institute (1960): *Recommended Practices for Core-analysis Procedure.* API Recommended Practice 40 (RP 40), 1st ed., American Petroleum Institute, Washington, D.C.

Bird, J. M., and Dewey, J. F. (1970): Lithosphere plate continental margin tectonics and the evolution of the Appalachian orogen. Geol. Soc. Am. Bull., v. 81, p. 1031-1060.

Dorsch, J. (1995): *Determination of effective porosity of mudrocks - A feasibility study.* ORNL/GWPO-019. Oak Ridge National Laboratory, Oak Ridge, Tenn.

Dorsch, J., Katsube, T. J., Sanford, E. E., Dugan, B. E., and Tourkow, L. (1996): *Effective porosity and pore-throat sizes of Conasauga Group mudrock: Application, test and evaluation of Petrophysical Techniques.* ORNL/GWPO-021. Oak Ridge National Laboratory, Oak Ridge, Tenn.

Dorsch, J., and Katsube, T. J. (1996): *Effective porosity and pore-throat sizes of mudrock saprolite from the Nolichucky Shale within Bear Creek Valley on the Oak Ridge Reservation: Implications for contaminant spread and retardation through matrix diffusion.* ORNL/GWPO-025. Oak Ridge National Laboratory, Oak Ridge, Tenn.

Dreier, R. B., Hatcher, R. D., Jr., Lietzke, D. A. (1992): 3.3 Conasauga Group. In: R. D. Hatcher, Jr., P. J. Lemiszki, R. B. Dreier, R. H. Ketelle, R. R. Lee, D. A. Lietzke, W. M. McMaster, J. L. Foreman, and S. Y. Lee: *Status Report on the geology of the Oak Ridge Reservation.* ORNL/TM-12074. Oak Ridge National Laboratory, Oak Ridge, Tenn., p. 18-41.

Füchtbauer, H., and Richter, D. K. (1988): Karbonatgesteine. In: Füchtbauer, H., ed., Sedimente und Sedimentgesteine. Schweizerbart, Stuttgart, p. 233-434.

Goldstrand, P. M. (1995): Stratigraphic variations and secondary porosity within the Maynardville Limestone in Bear Creek Valley, Y-12 Plant, Oak Ridge, Tennessee. Y/TS-1093. Oak Ridge Y-12 Plant, Oak Ridge, Tenn.

Goldstrand, P. M., Menefee, L. S., and Dreier, R. B. (1995): Porosity development in the Copper Ridge Dolomite and Maynardville Limestone, Bear Creek Valley and Chestnut Ridge, Tennessee. Y/SUB95-SP912V/1-1093. Oak Ridge Y-12 Plant, Oak Ridge, Tenn.

Goldstrand, P. M., and Shevenell, L. A. (1994): Lithologic controls on karst development and groundwater flow in the Copper Ridge and Maynardville Limestone, Oak Ridge, Tennessee. Geol. Soc. Am. Abstracts with Programs, v. 26, p. 204.

Hasson, K. O., and Haase, C. S. (1988): Lithofacies and paleogeography of the Conasauga Group (Middle and Late Cambrian) in the Valley and Ridge Province of East Tennessee. Geological Society of America Bulletin, v. 100, p. 234-246.

Hatcher, R. D., Jr., Lemiszki, P. J., Dreier, R. B., Ketelle, R. H., Lee, R. R., Lietzke, D. A., McMaster, W. M., Foreman, J. L., and Lee, S. Y. (1992a): *Status Report on the geology of the Oak Ridge Reservation.* ORNL/TM-12074. Oak Ridge National Laboratory, Oak Ridge, Tenn.

Hatcher, R. D., Jr., Lemiszki, P. J., and Lietzke, D. A. (1992b): 3.4 Knox Group. In: R. D. Hatcher, Jr., P. J. Lemiszki, R. B. Dreier, R. H. Ketelle, R. R. Lee, D. A. Lietzke, W. M. McMaster, J. L. Foreman, and S. Y. Lee: *Status Report on the geology of the Oak Ridge Reservation.* ORNL/TM-12074. Oak Ridge National Laboratory, Oak Ridge, Tenn., p. 41-50.

Katsube, T. J. (1992): Statistical analysis of pore-size distribution data of tight shales from the Scotian Shelf. In: *Current Research, Part E.* Geological Survey of Canada, Paper 91-1E, p. 365-372.

Katsube, T. J., and Scromeda, N. (1991): Effective porosity measuring procedure for low porosity rocks. In: *Current Research, Part E.* Geological Survey of Canada, Paper 91-1E, p. 291-297.

Katsube, T. J., Scromeda, N., and Williamson, M. (1992a): Effective porosity from tight shales from the Venture gas field, offshore Nova Scotia. In: *Current Research, Part D.* Geological Survey of Canada, Paper 92-1D, p. 111-119.

Katsube, T. J., Williamson, M., and Best, M. E. (1992b): Shale pore structure evolution and its effect on permeability. In: *Symposium Volume III of the Thirty-Third Annual Symposium of the Society of Professional Well Log Analysts (SPWLA).* The Society of Core Analysts Preprints, Oklahoma City, Oklahoma, Paper SCA-6214, p. 1-24.

King, H. L., and Haase, C. S. (1987): Subsurface-controlled geologic maps for the Y-12 Plant and adjacent areas of Bear Creek Valley. ORNL/TM-10112. Oak Ridge National Laboratory, Oak Ridge, Tenn.

Lee, R. R., and Ketelle, R. H. (1987): Stratigraphic influence on deep groundwater flow in the Knox Group Copper Ridge Dolomite on the west Chestnut Ridge site. ORNL/TM-10479. Oak Ridge National Laboratory, Oak Ridge, Tenn.

Luffel, D. L., and Howard, W. E. (1988): Reliability of laboratory measurement of porosity in tight gas sands. SPE Formation Evaluation, December, p. 705-710.

Miller, R. L., and Fuller, J. O. (1954): Geology and oil resources of the Rose Hill district - the fenster area of the Cumberland overthrust block, Lee County, Virginia. Virginia Geological Survey Bulletin 71.

Olhoeft, G. R., and Johnson, G. R. (1989): Densities of rocks and minerals. In: Carmichael, R. S., ed., *Practical Handbook of Physical Properties of Rocks and Minerals.* CRC Press, Boca Raton, p. 141-176.

Read, J. F. (1989): Controls on evolution of Cambrian-Ordovician passive margin, U.S. Appalachians. In: Crevello, P., Wilson, J. L., Sarg, J. F., and Read, J. F., eds., Controls on carbonate platform and basin development. SEPM Special Publication, v. 44, p. 147-166.

Rodgers, J. (1953): Geologic map of East Tennessee with explanatory text, scale 1:125 000. Tenn. Div. Geology Bull. 58, pt II.

Rodgers, J. (1969): The eastern edge of the North American continent during the Cambrian and Early Ordovician. In: Zen, E-an, White, W., Hadley, J., and Thompson, J., jr., eds., Studies of Appalachian Geology: Northern and Maritime. Interscience Publ., New York, p. 141-149.

Saunders, J. A., and Toran, L. E. (1994): Evidence for dedolomitization and mixing in Paleozoic carbonates near Oak Ridge, Tennessee. Ground Water, v. 32, p. 207-214.

Scromeda, N., and Katsube, T. J. (1993): Effect of vacuum-drying and temperature on effective porosity determination for tight rocks. In: *Current Research, Part E.* Geological Survey of Canada, Paper-1E, p. 313-319.

Scromeda, N., and Katsube, T. J. (1994): Effect of temperature on drying procedures used in porosity measurements of tight rocks. In: *Current Research, Part E.* Geological Survey of Canada, Paper-1E, p. 283-289.

Shevenell, L. M., Dreier, R. B., and Jago W. K. (1993): Summary of fiscal years 1991 and 1992 construction, hydrologic, and geological data obtained from the Maynardville Limestone exit pathway monitoring program. Y/TS-814. Oak Ridge National Laboratory, Oak Ridge, Tenn.

Solomon, D. K., Moore, G. K., Toran, L. E., Dreier, R. B., and McMaster, W. M. (1992): *Status report: A hydrologic framework for the Oak Ridge Reservation.* ORNL/TM-12026. Oak Ridge National Laboratory, Oak Ridge, Tenn., variously paginated.

Thomas, D. C., and Pugh, V. J. (1989): A statistical analysis of the accuracy and reproducibility of standard core analysis. The Log Analyst, v. (March-April 1989), p. 71-76.

Weber, L. J., Jr. (1988): Paleoenvironmental analysis and test of stratigraphic cyclicity in the Nolichucky Shale and Maynardville Limestone (Upper Cambrian) in central East Tennessee. Unpubl. Ph. D. Dissertation, University of Tennessee, Knoxville.

APPENDIX I: Sampling Intervals

Summary information on sampling locations of specimens: designation of sampling intervals, cores, core boxes, drill depths (below ground surface), and stratigraphic units from which specimens were obtained. Stratigraphic units are: **CR** refers to the Copper Ridge Dolomite of the Knox Group, whereas **MV** refers to the Maynardville Limestone of the Conasauga Group; numbers in parentheses for the Maynardville Limestone refer to the zonation (zones 1 through 7) of the Maynardville Limestone (following Shevenell et al., 1993; Goldstrand, 1995).

Sampl. int.	Core	Box	Drill depth	Strat. unit
131-42	131	42	419' 2" (127.76 m)	CR
131-44	131	44	442' 3" (134.80 m)	CR
131-45	131	45	449' 4" (136.96 m)	CR
131-49-1	131	49	487' 10" (148.69 m)	CR
131-49-2	131	49	489' 7" (149.23 m)	CR
131-50	131	50	497' 3" (151.56 m)	CR
131-51	131	51	506' 2" (154.28 m)	CR
131-53	131	53	523' 6" (159.56 m)	CR
131-58	131	58	574' 8" (175.16 m)	CR
131-60	131	60	587' 5" (179.05 m)	CR
131-61	131	61	602' 9" (183.72 m)	MV (6)
131-63	131	63	619' 10" (188.93 m)	MV (6)
131-65	131	65	641' 3" (195.45 m)	MV (6)
131-69-2	131	69	675' 7" (205.92 m)	MV (6)
131-69-1	131	69	677' (206.35 m)	MV (6)
131-73	131	73	712' (217.02 m)	MV (6)
131-78	131	78	758' 9" (231.27 m)	MV (5)
131-80	131	80	777' 2" (236.88 m)	MV (5)
131-84	131	84	814' 6" (248.26 m)	MV (4)
131-87	131	87	848' 6" (258.62 m)	MV (4)
131-90	131	90	873' 7" (266.27 m)	MV (4)
131-91	131	91	880' 2" (268.28 m)	MV (4)
131-98	131	98	951' 7" (290.04 m)	MV (3)
131-100	131	100	966' (294.44 m)	MV (3)
131-102	131	102	989' 6" (301.60 m)	MV (3)
131-106	131	106	1022' 2" (311.56 m)	MV (2)
131-111	131	111	1071' 2" (326.49 m)	MV (2)
131-113	131	113	1094' 6" (333.60 m)	MV (2)

Sampl. int.	Core	Box	Drill depth	Strat. unit
135-48	135	48	511' 4" (155.85 m)	CR
135-56	135	56	583' 3" (177.78 m)	CR
135-58	135	58	605' 5" (184.53 m)	CR
135-59	135	59	611' (186.23 m)	CR
135-60	135	60	622' 6" (189.74 m)	CR
135-61	135	61	633' 6" (193.09 m)	CR
135-64	135	64	664' 4" (202.49 m)	CR
135-68	135	68	696' 4" (212.24 m)	MV (6)
135-72	135	72	732' (223.11 m)	MV (6)
135-73	135	73	745' 7" (227.25 m)	MV (6)
135-76	135	76	769' 2" (234.44 m)	MV (6)
135-79	135	79	798' 9" (243.46 m)	MV (6)
135-81	135	81	818' 8" (249.53 m)	MV (5)
135-83	135	83	837' 11" (255.40 m)	MV (5)
135-88	135	88	882' 3" (268.91 m)	MV (4)
135-95	135	95	953' 2" (290.53 m)	MV (4)
135-101	135	101	1005' 10" (306.58 m)	MV (3)
135-104	135	104	1033' 4" (314.96 m)	MV (3)
135-105	135	105	1043' 4" (318.01 m)	MV (3)
135-107	135	107	1063' 3" (324.08 m)	MV (2)
135-115	135	115	1133' 6" (345.49 m)	MV (2)
135-121	135	121	1197' 7" (365.02 m)	MV (2)

APPENDIX II: Results - Specimen Densities

Summary of bulk-density and grain-density data for carbonate-rock specimens from the Maynardville Limestone and Copper Ridge Dolomite, Bear Creek Valley on the ORR. Specimen grain-density was determined during helium porosimetry, whereas specimen bulk-density was determined by immersion in mercury (Archimedes principle).

Specimen	δ_{grain} [g/cc]	δ_{bulk} [g/cc]
131-42-A	2.83	2.82
131-44-A	2.82	2.81
131-45-A	2.82	2.79
131-49-A1	2.83	2.75
131-49-A2	2.84	2.80
131-50-A	2.86	2.79
131-51-A	2.79	2.73
131-53-A	2.80	2.77
131-58-A	2.84	2.79
131-60-A	2.81	2.79
131-61-A	2.82	2.81
131-63-A	2.70	2.69
131-65-A	2.78	2.75
131-69-A1	2.85	2.62
131-69-A2	2.78	2.75
131-73-A	2.71	2.70
131-78-A	2.73	2.72
131-80-A	2.71	2.71
131-84-A	2.72	2.72
131-87-A	2.71	2.70
131-90-A	2.71	2.70
131-91-A	2.76	2.75
131-98-A	2.73	2.73
131-100-A	2.72	2.72
131-102-A	2.72	2.72
131-106-A	2.72	2.71
131-111-A	2.71	2.70
131-113-A	2.71	2.71
135-48-A	2.84	2.83
135-56-A	2.83	2.81
135-58-A	2.79	2.78
135-59-A	2.80	2.76
135-60-A	2.83	2.80
135-61-A	2.82	2.78
135-64-A	2.87	2.72
135-68-A	2.74	2.73
135-72-A	2.84	2.75
135-73-A	2.84	2.72
135-76-A	2.84	2.79
135-79-A	2.70	2.70
135-81-A	2.76	2.75
135-83-A	2.70	2.69
135-88-A	2.75	2.75
135-95-A	2.75	2.74
135-101-A	2.74	2.73
135-104-A	2.70	2.70
135-105-A	2.74	2.72
135-107-A	2.71	2.70
135-115-A	2.71	2.70
135-121-A	2.73	2.73

APPENDIX III: Statistical Measures - Specimen Densities

Some statistical measures for specimen bulk-density and specimen grain-density calculated for Maynardville Limestone and Copper Ridge Dolomite from Bear Creek Valley on the ORR. Density measures are in $g \cdot cm^{-3}$. Abbreviations: **x** = arithmetic mean, **sx** = standard deviation, **n** = number of specimen analyses; **units** refers to analyzed stratigraphic units, MV-6, etc. refers to the analyzed stratigraphic zones within the Maynardville Limestone.

Unit or Zone	Core	Grain Density			Bulk Density		
		x	sx	n	x	sx	n
All units	GW-131 & GW-135	2.77	0.06	50	2.74	0.04	50
	GW-131	2.77	0.06	28	2.74	0.05	28
	GW-135	2.77	0.06	22	2.75	0.04	22
Copper	GW-131 & GW-135	2.83	0.02	17	2.78	0.03	17
Ridge	GW-131	2.82	0.02	10	2.78	0.03	10
Dolomite	GW-135	2.83	0.03	7	2.78	0.04	7
Maynardville	GW-131 & GW-135	2.74	0.05	33	2.72	0.03	33
Limestone	GW-131	2.74	0.04	18	2.72	0.04	18
	GW-135	2.75	0.05	15	2.73	0.03	15
MV-6	GW-131 & GW-135	2.78	0.06	11	2.73	0.05	11
	GW-131	2.77	0.06	6	2.72	0.07	6
	GW-135	2.79	0.07	5	2.74	0.03	5
MV-5	GW-131 & GW-135	2.73	0.03	4	2.72	0.03	4
	GW-131	2.72	0.01	2	2.72	0.01	2
	GW-135	2.73	0.04	2	2.72	0.04	2
MV-4	GW-131 & GW-135	2.73	0.02	6	2.73	0.02	6
	GW-131	2.73	0.02	4	2.72	0.02	4
	GW-135	2.75	0.00	2	2.75	0.01	2
MV-3	GW-131 & GW-135	2.73	0.02	6	2.72	0.01	6
	GW-131	2.72	0.01	3	2.72	0.01	3
	GW-135	2.73	0.02	3	2.72	0.02	3
MV-2	GW-131 & GW-135	2.72	0.01	6	2.71	0.01	6
	GW-131	2.71	0.01	3	2.71	0.01	3
	GW-135	2.72	0.01	3	2.71	0.02	3

APPENDIX IV: Results - Specimen Effective Porosity (Helium Porosimetry)

Summary of effective porosity data for carbonate-rock specimens from the Maynardville Limestone and Copper Ridge Dolomite, Bear Creek Valley on the ORR, based on helium porosimetry.

Specimen	ϕHe[%]
131-42-A	0.59
131-44-A	0.22
131-45-A	1.13
131-49-A1	2.77
131-49-A2	1.25
131-50-A	2.40
131-51-A	2.17
131-53-A	1.19
131-58-A	1.62
131-60-A	0.81
131-61-A	0.45
131-63-A	0.61
131-65-A	1.12
131-69-A1	8.13
131-69-A2	1.06
131-73-A	0.37
131-78-A	0.37
131-80-A	0.22
131-84-A	0.22
131-87-A	0.37
131-90-A	0.37
131-91-A	0.45
131-98-A	0.22
131-100-A	0.22
131-102-A	0.30
131-106-A	0.52
131-111-A	0.22
131-113-A	0.22

Specimen	ϕHe [%]
135-48-A	0.21
135-56-A	0.48
135-58-A	0.55
135-59-A	1.47
135-60-A	0.92
135-61-A	1.53
135-64-A	4.99
135-68-A	0.10
135-72-A	3.34
135-73-A	4.10
135-76-A	1.79
135-79-A	0.10
135-81-A	0.46
135-83-A	0.34
135-88-A	0.28
135-95-A	0.36
135-101-A	0.24
135-104-A	0.14
135-105-A	0.56
135-107-A	0.17
135-115-A	0.15
135-121-A	0.06

APPENDIX V: Results - Specimen Effective Porosity (Immersion-Saturation Method)

Summary of effective porosity data for carbonate-rock specimens from the Maynardville Limestone and Copper Ridge Dolomite, Bear Creek Valley on the ORR, based on the immersion-saturation method.

Specimen	W_{SAT}[g]	W_{DRY} [g]	ΔW [g]	δ bulk [g/cc]	ϕ_{IMS}[%]
131-42-C	16.5882	16.5281	0.0601	2.815	1.02
131-44-C	16.3077	16.2755	0.0322	2.814	0.56
131-45-C	15.1511	15.0809	0.0702	2.791	1.30
131-49-1-C	16.3253	16.2178	0.1075	2.749	1.82
131-49-2-C	16.2381	16.1786	0.0595	2.801	1.03
131-50-C	15.2872	15.1548	0.1324	2.787	2.43
131-51-C	15.3844	15.1831	0.2013	2.730	3.62
131-53-C	15.6250	15.5105	0.1145	2.767	2.04
131-58-C	16.0833	15.9888	0.0945	2.790	1.65
131-60-C	15.8648	15.8340	0.0308	2.788	0.54
131-61-C	15.1273	15.1033	0.0240	2.808	0.45
131-63-C	14.6175	14.5883	0.0292	2.687	0.54
131-65-C	15.4515	15.4021	0.0494	2.748	0.88
131-69-1-C	14.9417	14.6879	0.2538	2.617	4.52
131-69-2-C	15.0103	14.9741	0.0362	2.751	0.67
131-73-C	14.9219	14.9086	0.0133	2.698	0.24
131-78-C	15.1130	15.1007	0.0123	2.723	0.22
131-80-C	14.9159	14.9043	0.0116	2.707	0.21
131-84-C	17.5260	17.4332	0.0928	2.716	1.45
131-87-C	15.5708	15.5584	0.0124	2.698	0.22
131-90-C	14.7446	14.7276	0.0170	2.703	0.31
131-91-C	14.6207	14.6042	0.0165	2.748	0.31
131-98-C	14.9134	14.9042	0.0092	2.726	0.17
131-100-C	16.0075	15.9904	0.0171	2.716	0.29
131-102-C	15.3241	15.3071	0.0170	2.715	0.30
131-106-C	15.4913	15.4559	0.0354	2.707	0.62
131-111-C	15.3200	15.2952	0.0248	2.702	0.44
131-113-C	14.5153	14.4879	0.0274	2.710	0.51
135-48-D	14.7566	14.7390	0.0176	2.833	0.34
135-56-C	14.8917	14.8490	0.0427	2.814	0.81
135-58-C	15.7049	15.6079	0.0970	2.775	1.72
135-59-B	35.4826	35.0979	0.3847	2.756	3.02
135-59-D	16.2574	16.0941	0.1633	2.756	2.80
135-60-D	13.0584	12.9938	0.0646	2.800	1.39
135-61-B	35.5704	35.3605	0.2099	2.780	1.65
135-61-D	12.6961	12.6068	0.0893	2.780	1.97
135-64-C	18.6586	18.4282	0.2304	2.724	3.41
135-68-C	15.4939	15.4804	0.0135	2.734	0.24
135-72-B	36.6444	36.4358	0.2086	2.749	1.57
135-72-D	16.0037	15.8436	0.1601	2.749	2.78
135-73-B	36.5996	36.3929	0.2067	2.724	1.55
135-73-D	15.6417	15.5811	0.0606	2.724	1.06
135-76-C	14.1282	14.0354	0.0928	2.789	1.84
135-79-C	14.4870	14.4795	0.0075	2.697	0.14
135-81-C	17.9132	17.8977	0.0155	2.745	0.24
135-83-B	34.7544	34.7133	0.0411	2.694	0.32
135-83-D	12.6318	12.6203	0.0115	2.694	0.25
135-88-B	36.0565	36.0281	0.0284	2.746	0.22
135-88-D	15.4607	15.4438	0.0169	2.746	0.30
131-95-D	15.0226	15.0067	0.0159	2.740	0.29
135-101-B	35.7358	35.7016	0.0342	2.731	0.26
135-101-D	13.8478	13.8351	0.0127	2.731	0.25
135-104-D	13.0179	13.0064	0.0115	2.700	0.24
135-105-B	35.0688	35.0388	0.0300	2.721	0.23
131-105-D	14.0240	14.0061	0.0179	2.721	0.35
131-107-D	14.2451	14.2134	0.0317	2.703	0.60
135-115-B	35.5611	35.4979	0.0632	2.704	0.48
135-115-D	13.8305	13.8084	0.0221	2.704	0.43
135-121-B	35.9623	35.9269	0.0354	2.725	0.27
135-121-D	16.0395	16.0153	0.0242	2.725	0.41

APPENDIX VI: Statistical Measures - Specimen Effective Porosity

Some statistical measures for specimen effective porosities (based on helium porosimetry and the immersion-saturation method) calculated for the Maynardville Limestone and Copper Ridge Dolomite, Bear Creek Valley on the ORR. Effective porosity measures are in %. Abbreviations: x = arithmetic mean, sx = standard deviation, n = is number of specimen analyses; **units** refers to analyzed stratigraphic units, **MV-6**, etc. refers to the analyzed stratigraphic zones within the Maynardville Limestone.

Unit or Zone	Core	He-porosity			Immers.-sat.-porosity		
		x	sx	n	x	sx	n
All Units	GW-131 & GW-135	1.04	1.47	50	1.00	1.00	60
	GW-131	1.06	1.56	28	1.01	1.06	28
	GW-135	1.02	1.39	22	0.98	0.97	32
Copper	GW-131 & GW-135	1.43	1.18	17	1.74	0.96	19
Ridge	GW-131	1.42	0.82	10	1.60	0.94	10
Dolomite	GW-135	1.45	1.64	7	1.90	1.02	9
Maynardville	GW-131 & GW-135	0.84	1.58	33	0.65	0.83	41
Limestone	GW-131	0.86	1.83	18	0.69	1.01	18
	GW-135	0.81	1.26	15	0.62	0.68	23
MV-6	GW-131 & GW-135	1.93	2.44	11	1.27	1.24	13
	GW-131	1.96	3.04	6	1.22	1.63	6
	GW-135	1.89	1.83	5	1.31	0.93	7
MV-5	GW-131 & GW-135	0.35	0.10	4	0.25	0.04	5
	GW-131	0.30	0.11	2	0.22	0.01	2
	GW-135	0.40	0.09	2	0.27	0.04	3
MV-4	GW-131 & GW-135	0.34	0.08	6	0.44	0.45	7
	GW-131	0.35	0.10	4	0.57	0.59	4
	GW-135	0.32	0.06	2	0.27	0.04	3
MV-3	GW-131 & GW-135	0.28	0.15	6	0.26	0.05	8
	GW-131	0.25	0.05	3	0.25	0.07	3
	GW-135	0.31	0.22	3	0.26	0.05	5
MV-2	GW-131 & GW-135	0.22	0.16	6	0.47	0.11	8
	GW-131	0.32	0.17	3	0.52	0.09	3
	GW-135	0.13	0.06	3	0.44	0.12	5

APPENDIX VII: Equivalent Porosity Data (from Goldstrand et al., 1995)

Comparison of selected effective porosities obtained during this study with equivalent porosities as determined by Goldstrand et al. (1995). Depths are given as below ground surface. Abbreviations: **sampl. int.** refers to sampling intervals of this study, **He** refers to helium-porosimetry data, whereas **IMS** refers to effective porosity data obtained with the immersion-saturation method; **G** refers to data obtained by Goldstrand et al. (1995); the asterisks indicates that the porosities are mean values (calculated from several - two to three - separate values), **N.A.** refers to non-availability of respective data.

Sampling Interval	Current Study			Goldstrand Study		
	Depth	ϕHe [%]	ϕIMS [%]	Depth	ϕG-IMS [%]	ϕG-petr [%]
135-58	605' 5" (184.53 m)	0.55	1.72	605' (184.40 m)	0.3*	N.A.
135-59	611' (186.23 m)	1.47	2.91*	611' (186.23 m)	0.5*	N.A.
135-61	633' 6" (193.09 m)	1.53	1.81*	634' 5" (193.37 m)	1.0*	N.A.
135-64	664' 4" (202.49 m)	4.99	3.41	665' (202.69 m)	1.3*	N.A.
135-68	696' 4" (212.24 m)	0.10	0.24	697' 6" (212.60 m)	0.3*	N.A.
135-72	732' (223.11 m)	3.34	2.18*	731' 6" (222.96 m)	1.4*	1.6
135-73	745' 7" (227.25 m)	4.10	1.31*	745' (227.08 m)	2.3*	1.3
135-76	769' 2" (234.44 m)	1.79	1.84	769' (234.39 m)	1.7*	10.3
135-79	798' 9" (243.46 m)	0.10	0.14	798' (243.23 m)	1.2*	N.A.
135-81	818' 8" (249.53 m)	0.46	0.24	817' 6" (249.17 m)	0.4*	0.0
135-83	837' 11" (255.40 m)	0.34	0.29*	837' 6" (255.27 m)	2.3*	0.0
135-88	882' 3" (268.91 m)	0.28	0.26*	882' 6" (268.99 m)	0.2*	0.0
135-95	953' 2" (290.53 m)	0.36	0.29	953' (290.47 m)	0.8*	0.0
135-101	1005' 10" (306.58 m)	0.24	0.26*	1006' (306.63 m)	0.4*	0.0
135-104	1033' 4" (314.96 m)	0.14	0.24	1033' (314.86 m)	0.3*	N.A.
135-105	1043' 4" (318.01 m)	0.56	0.29*	1044' (318.21 m)	0.2*	0.0
135-107	1063' 3" (324.08 m)	0.17	0.60	1063' (324.00 m)	0.4*	N.A.
135-115	1133' 6" (345.49 m)	0.15	0.46*	1133' (345.34 m)	0.2*	0.0
135-121	1197' 7" (365.02 m)	0.06	0.34*	1198' (365.15 m)	0.3*	0.3

Internal Distribution

1. L. D. Bates, 1001, MS-7169
2. F. P. Baxter, 3504, MS-6317
3. H. L. Boston, 4500-N, MS-6200
4. H. M. Braunstein, 130 MIT, MS-6282
5. A. J. Caldanaro, 1509, MS-6400
6. B. J. Carr, 1509, MS-6400
7. K. W. Cook, 1330, MS-7298
8. T. L. Cothron, C-72
9. N. H. Cutshall, C207, MS-7172
10. M. F. P. DeLozier, 1037, MS-7355
11. A. F. Diefendorf, 1509, MS-6400
12. W. E. Doll, 1509, MS-6400

13-19. J. Dorsch, 1509, MS-6400

20. R. B. Dreier, 1509, MS-6400
21. T. O. Early, 1509, MS-6400
22. J. M. Forstrom, 0303-8, MS-7314
23. C. W. Francis, 3504, MS-6317
24. D. W. Frazier, 4500-N, MS-6198
25. S. B. Garland, II, 7078-B, MS-6402
26. C. W. Gehrs, 1505, 6036
27. P. L. Goddard, 1330, MS-7298
28. J.-P. Gwo, 4500-N, MS-6203
29. S. C. Haase, 1330, MS-7298
30. R. D. Hatcher, Jr., 1509, MS-6400
31. Lucius Holder, Jr., 3001, MS-6029
32. D. D. Huff, 1509, MS-6400
33. G. K. Jacobs, 1505, MS-6036
34. W. K. Jago, 9207, MS-8225
35. P. M. Jardine, 1505, MS-6038
36. J. A. Johnston, Jr., 9983-58, MS-8247
37. S. B. Jones, 9207, MS-8225
38. R. H. Ketelle, 4500N, MS-6185
39. B. L. Kimmel, 4500-S, MS-6125
40. A. J. Kuhaida, 7078-B, MS-6402
41. R. R. Lee, 4500-N, MS-6185
42. S. Y. Lee, 1505, MS-6038
43. R. J. Luxmoore, 1505, MS-6038
44. J. F. McCarthy, 1505, MS-6036
45. L. W. McMahon, 9116, MS-8098
46. G. R. Moline, 1509, MS-6400
47. P. J. Mulholland, 1505, MS-6036
48. J. B. Murphy, 4500-N, MS-6198
49. C. E. Nix, 6026-C, MS-6395
50. M. J. Norris, 9983-AH, MS-8247
51. J. E. Nyquist, 1509, MS-6400
52. F. S. Patton, Jr., 1001-B, MS-7169
53. T. Purucker, 105 MIT, MS-6452
54. C. T. Rightmire, 1509, MS-6400
55. T. H. Row, 4500-N, MS-6254
56. F. E. Sharples, 1505, MS-6036
57. L. G. Shipe, 0303-8, MS-7314
58. R. L. Siegrist, 1505, MS-6038
59. E. D. Smith, 1505, MS-6038
60. M. F. Tardiff, 4500-N, MS-6198
61. L. E. Toran, 1509, MS-6400
62. J. R. Trabalka, 3047, MS-6020
63. J. C. Wang, 4500-N, MS-6185
64. D. R. Watkins, 3504, MS-6317

65-69. D. B. Watson, 1509, MS-6400

70. T. F. Zondlo, 1509, MS-6400
71. Central Research Library

72-74. Lab Records-RC

External Distribution

75. Jerry Archer, Jacobs Engineering, 125 Broadway Ave. Oak Ridge, TN 37830

76. Richard Arnseth, SAIC, 301 Laboratory Rd., Oak Ridge, TN 37830

77. Ernest Beauchamp, C-260 Jackson Plaza, MS-7614, R13, Oak Ridge, TN 37830

78. Robert Benfield, TDEC/DOE Oversight, 761 Emory Valley Rd., Oak Ridge, TN 37830

79. J. Blount, Jacobs Engineering, 125 Broadway Ave. Oak Ridge, TN 37830

80. G. W. Bodenstein, USDOE-OR Federal Bldg., Oak Ridge, TN 37830

81. H. L. Boston, Lockheed Martin Corporation, Hanford, 2950 George Washington Way, Richland, WA 99352

82. M. Broido, Acting Director, Environmental Sciences Division, ER-74, Department of Energy, 19901 Germantown Road, Germantown, MD 20874

83. Don Byerly, Department of Geological Sciences, University of Tennessee, Knoxville, TN 37996

84. Paul Craig, Environmental Consulting Engineers, P.O. Box 22668, Knoxville, TN 37933

85. S. N. Davis, 6540 Box Canyon Drive, Tucson, AZ 85745

86. Director, Center for Management, Utilization, and Protection of Water Resources, Tennessee Technological University, P.O. Box 5082, Cookeville, TN 38505

87. F. A. Donath, Director, Institute for Environmental Education, Geological Society of America, 1006 Las Posas, San Clemente, CA 92673

88. S. G. Driese, Department of Geological Sciences, University of Tennessee, Knoxville, TN 37996

89. W. M. Dunne, Department of Geological Sciences, University of Tennessee, Knoxville, TN 37996

90. E. Evans, Jacobs Engineering, 125 Broadway Ave. Oak Ridge, TN 37830

91. J. L. Foreman, Exxon Production Research Co., P. O. Box 2189, Houston, TX 77252-2189

92. J. F. Franklin, College of Forest Resources, Anderson Hall AR-10, University of Washington, Seattle, WA 98185

93. D. W. Freckman, Director, College of Natural Resources, 101 Natural Resources Building, Colorado State University, Fort Collins, CO 80523

94. P. M. Goldstrand, Department of Geological Sciences, MS-172, University of Nevada, Reno, NV 89557

95. Jim Harless, TDEC/DOE Oversight, 761 Emory Valley Rd., Oak Ridge, TN 37830

96. R. C. Harriss, Institute for the Study of Earth, Oceans, and Space, University of New Hampshire, Durham, NH 03824

97. P. Hoffmann, Department of Energy, 3 Main St., Oak Ridge, TN 37830

98. G. M. Hornberger, Dept. of Environmental Sciences, University of Virginia, Charlottesville, VA 22903

99. R. O. Hultgren, ORNL Site Manager, Department of Energy, Oak Ridge National Laboratory, P. O. Box 2008, Oak Ridge, TN 37831-6269

100. G. Y. Jordy, Office of Program Analysis, Office of Energy Research, ER-30, G-226, USDOE, Washington, D.C. 20545

101-102. H. E. Julian, TVA Engineering Laboratory, PO Drawer E, Norris, TN 37828

103. T. J. Katsube, Geological Survey of Canada, Mineral Resources Division, 601 Booth Street, Ottawa, Ontario, CANADA K1A 0E8

104. A. Khan, SAIC, 301 Laboratory Rd., Oak Ridge, TN 37830

105. D. C. Kopaska-Merkel, Geological Survey of Alabama, 420 Hackberry Lane, Tuscaloosa, AL 35486

106. O. C. Kopp, Department of Geological Sciences, University of Tennessee, Knoxville, TN 37996

107. P. E. Lamoreaux & Assoc. Inc., P.O. Box 2310, Tuscaloosa, AL 35403

108. P. J. Lemiszki, Department of Geological Sciences, University of Tennessee, Knoxville, TN 37996

109. D. A. Lietzke, Lietzke Soil Services, Route 3, Box 607, Rutledge, TN 37861

110. Changsheng Lu, Jacobs ER Team, 125 Broadway Ave. Oak Ridge, TN 37830

111. C. T. Lutz, CDM Federal, 800 Oak Ridge Turnpike, Oak Ridge TN 37830

112-114. L. D. McKay, Department of Geological Sciences, University of Tennessee, Knoxville, TN 37996

115. W. M. McMaster, Dept. of Civil Engineering, University of Tennessee, 62 Perkins Hall, Knoxville, TN 37996-2010

116. Manager, CH2M Hill, 599 Oak Ridge Turnpike, Oak Ridge, TN 37830

117. G. K. Moore, Route 4, Box 927, Waynesboro, TN 38485

118. D. Moss, SAIC, 301 Laboratory Rd., Oak Ridge, TN 37830

119. Ronit Nativ, Dept. of Soil and Water Sci., Faculty of Agriculture, Hebrew University of Jerusalem, P.O. Box 12, Rehovot 76100, ISRAEL

120. Chudi Nwangwa, TDEC/DOE Oversight, 761 Emory Valley Rd., Oak Ridge, TN 37830

121. R. H. Olsen, Microbiology & Immunology Dept., University of Michigan, Medical Sciences II, #5605, 1301 East Catherine St., Ann Arbor, MI 48109-0620

122. A. Patrinos, Associate Director, Office of Health & Environmental Research, ER-70, Department of Energy, 19901 Germantown Road, Germantown, MD 20874

123. R. Pawlowicz, Bechtel, 151 Lafayette Dr. Oak Ridge, TN 37830

124. C. Provost, CDM Federal, 800 Oak Ridge Turnpike, Oak Ridge TN 37830

125. F. Quinones, Chief, Tennessee District, WRD, U.S. Geological Survey, 810 Broadway, Suite 500, Nashville, TN 37203

126. G. D. Reed, Dept. of Civil Engineering, University of Tennessee, 62 Perkins Hall, Knoxville, TN 37996-2010

127. W. E. Sanford, Dept. of Earth Resources, Colorado State University, Fort Collins, CO 80523-1482

128. G. S. Sayler, 10515 Research Drive, Suite 100, University of Tennessee, Knoxville, TN 37932-2567

129. D. Shults, Tennessee Dept. of Environment and Conservation, Div. of Radiological Health, TERRA Bldg., 150 Ninth Ave. North, Nashville, TN 37243-1532

130. W. C. Sidle, Environmental Protection Division, USDOE-OR, P.O. Box 2001, Oak Ridge, TN 37831-8739

131. J. Smoot, Dept. of Civil Engineering, University of Tennessee, 62 Perkins Hall, Knoxville, TN 37996-2010

132-133. D. K. Solomon, 2381 Beacon Drive, Salt Lake City, Utah 84108

134. D. A. Stephenson, South Pass Resources, Inc., 8669 East San Alberto Drive, Suite 101, Scottsdale, AZ 85258

135. M. Travaglini, Department of Energy, 3 Main St., Oak Ridge, TN 37830

136. B. A. Tschantz, Dept. of Civil Engineering, University of Tennessee, 62 Perkins Hall, Knoxville, TN 37996-2010

137. K. R. Walker, Department of Geological Sciences, University of Tennessee, Knoxville, TN 37996

138. W. White, 542 Glenn Road, State College, PA 16803

139. F. J. Wobber, Environmental Sciences Division, Office of Health & Environmental Research, Office of Energy Research, ER-74, USDOE, Washington, D.C. 20585

140. J. Young, Camp Dresser & McGee, Suite 500, 800 Oak Ridge Turnpike, Oak Ridge, TN 37830

141-142. S. C. Young, Environmental Consulting Engineers, P. O. Box 22668, Knoxville, TN 37933

143. Office of Assistant Manager for Energy Research & Development, USDOE-OR, P.O. Box 2001, Oak Ridge, TN 37831-8600

144-145. Office of Scientific & Technical Information, P.O. Box 62, Oak Ridge, TN 37831